World Electric Vehicle Journal

MDPI

Article

GIS-Based Multi-Criteria Optimization of EV Charging Stations Integrated into Public Lighting Infrastructure

Jurica Perko [1,*] and Danijel Topić [2]

[1] European Climate, Infrastructure and Environment Executive Agency, 1040 Brussels, Belgium
[2] Faculty of Electrical Engineering, Computer Science and Information Technology Osijek, 31000 Osijek, Croatia; danijel.topic@ferit.hr
* Correspondence: jurica.perko@ec.europa.eu

Abstract

The rapid growth of electric vehicle (EV) adoption requires the scalable and cost-effective deployment of publicly accessible charging infrastructure, where cost-effectiveness is understood in terms of infrastructure reuse rather than explicit economic optimisation. Integrating slow AC charging units into existing public lighting networks represents a promising infrastructure reuse strategy, though spatial feasibility, electrical constraints, and regulatory requirements must be addressed. This study proposes an integrated GIS–MCDA–MILP framework for the optimal allocation of EV charging stations within public lighting systems. GIS-based spatial analysis identifies feasible poles based on parking accessibility and demand indicators, while MCDA ranks candidate locations and a MILP model determines optimal deployment under capacity constraints and phased rollout scenarios. The framework also incorporates AFIR-based policy benchmarking to assess compliance under current and future EV adoption levels. A real-world case study identifies 1223 feasible poles with a structural hosting capacity of 368 chargers. The results demonstrate that such integration is viable at the spatial and cabinet-capacity planning level but structurally limited, with a critical fleet growth multiplier of approximately 3.4 identified as the threshold beyond which lighting-integrated deployment alone becomes insufficient for AFIR compliance. The proposed framework advances the state of practice by coupling spatial, electrical, and regulatory analysis within a single reproducible methodology, offering a transferable decision-support tool for sustainable urban EV charging planning.

Keywords: electric vehicles; charging stations; public lighting; GIS; multi-criteria decision analysis; mixed-integer linear programming; hosting capacity; AFIR; urban energy planning

Check for updates

Academic Editor: Peter Van den Bossche

Received: 27 April 2026
Revised: 13 May 2026
Accepted: 18 May 2026
Published: 21 May 2026

Copyright: © 2026 by the authors. Published by MDPI on behalf of the World Electric Vehicle Association. Licensee MDPI, Basel, Switzerland. This article is an open access article distributed under the terms and conditions of the Creative Commons Attribution (CC BY) license.

1. Introduction

The rapid growth of electric vehicle (EV) adoption has intensified the need for a scalable and cost-effective deployment of a publicly accessible charging infrastructure [1,2]. In response, the European Commission has introduced regulatory frameworks to accelerate infrastructure expansion, most notably the Alternative Fuels Infrastructure Regulation (AFIR) (EU) 2023/1804, which establishes mandatory national targets for publicly accessible charging stations across the Trans-European Transport Network (TEN-T) and urban areas. These requirements highlight the urgency of developing efficient deployment strategies that minimize infrastructure investment while ensuring accessibility and compliance. Effective from April 2024, this regulation requires that:

- For every battery electric light-duty vehicle (BEV), a total power output of at least 1.3 kW must be available through public charging stations;
- For plug-in hybrid vehicles (PHEV), a minimum of 0.8 kW of charging power must be provided;
- Distance-based targets ensure adequate EV charging coverage across major highways and urban areas [3].

Integration of EV charging stations into public lighting infrastructure is a cost-effective solution that can help achieve these mandatory targets with minimal investment in new infrastructure. In this context, cost-effectiveness refers specifically to the avoidance of dedicated civil works, new cable trenching, and separate grid connections required for standalone charging deployment. A formal quantification of the resulting cost savings is beyond the scope of this study and is identified as a direction for future research. However, this approach requires compliance with two key conditions:

1. Public lighting poles must be located near parking spaces to enable convenient vehicle access;
2. Charging stations should be positioned at a reasonable distance from multi-apartment buildings or other points of interest, ensuring accessibility for residents without dedicated home charging.

The optimal allocation of public EV charging stations in urban areas must consider EV user behaviour and charging demand, infrastructure costs and profitability, and integration with urban infrastructure.

EV users' travel behaviour and charging demand depend on three key factors: (1) charging availability, including accessibility and convenience, which significantly impact the likelihood of charging station use; (2) comfortable range, where EV users plan trips based on battery charge levels and the distance to the next available charging station; and (3) trip completion requirements, where the need to charge depends on the total trip distance and intermediate stops [4,5]. Several studies have applied clustering techniques to group users with similar charging behaviours, aiding in the strategic planning of charging station placement [6,7]. These papers propose location models that integrate EV drivers' existing activity patterns, suggesting that charging stations should be placed at locations where users already stop for other purposes (e.g., shopping centers, workplaces). This activity-based approach improves convenience and utilization rates. Additionally, recent research has incorporated machine learning and big data analytics to model EV user charging preferences, improving station allocation strategies [8].

Alongside user convenience, the financial viability of EV charging stations is a key concern [9]. It includes three main components: (1) installation costs, which vary significantly based on location and grid access; (2) profit maximization, as charging stations must be financially sustainable, considering both supplier investments and grid operator profitability [10–12]; and (3) dynamic pricing models, which optimize charging station use by adjusting costs based on demand and grid load [13,14].

Recent studies have proposed optimization models that balance installation costs, expected revenue, and grid impact using Genetic Algorithms (GA), Particle Swarm Optimization (PSO), and Mixed-Integer Linear Programming (MILP) [15–19].

Recent research has explored the integration of renewable energy sources to enhance the sustainability and self-sufficiency of EV charging infrastructure. A study introduces a novel Rank-Weigh-Rank (RWR) optimization algorithm for selecting optimal solar panel configurations to power EV parking lots. The findings demonstrate that incorporating photovoltaic (PV) systems can significantly reduce power losses in the distribution network while improving the energy efficiency of charging infrastructure. This approach aligns with strategies for optimizing the allocation of public EV charging stations, as integrating PV

solutions into public lighting infrastructure could further enhance the cost-effectiveness and energy independence of urban EV charging networks. This would help mitigate concerns about grid load constraints and peak-hour energy demands, which remain critical challenges in large-scale EV charging deployment. By incorporating distributed energy resources, such as solar-powered charging units, the overall financial viability and environmental sustainability of public EV charging infrastructure could be improved, aligning with broader efforts to reduce reliance on the central grid and promote decentralized energy solutions [20].

Integrating EV charging stations into public lighting infrastructure presents a unique challenge [1,21], as it requires urban planning coordination to ensure that stations are installed in locations with sufficient space, accessibility, and energy supply. Additionally, power system capacity assessments are necessary since public lighting systems were not originally designed for vehicle charging, making the development of load management strategies essential [10,11]. A GIS-based methodology has been widely adopted for spatial analysis of charging station locations. The European Commission has previously piloted such an approach in Bolzano, Italy, identifying high-priority locations for charging station deployment [22].

However, existing approaches often fail to simultaneously capture the interaction between spatial feasibility constraints and infrastructure-level electrical limitations, particularly at the level of public lighting networks. Although GIS-based spatial allocation models have been widely explored, electrical constraints are often incorporated at the feeder or network level, rather than at the level of specific infrastructure nodes such as public lighting cabinets [2].

In particular, the distinction between theoretical electrical capacity and effective structural hosting capacity, determined by the interaction between spatially feasible pole locations and cabinet-level capacity limits, remains insufficiently examined. As a result, many allocation models may overestimate realizable deployment potential by neglecting the spatial–electrical coupling inherent in infrastructure reuse.

Furthermore, regulatory benchmarking frameworks such as AFIR are rarely integrated into infrastructure allocation models as quantitative evaluation layers. Consequently, there is a lack of methodologies capable of simultaneously capturing [3]:

- GIS-based spatial feasibility of candidate poles;
- Cabinet-level electrical constraints;
- Structural hosting limits under spatial restrictions;
- Regulatory adequacy under projected EV growth.

To address this gap, this study proposes an integrated GIS–MCDA–MILP framework for the optimal allocation of EV charging stations embedded within public lighting infrastructure. The aim of this study is to provide a spatially and electrically consistent decision-support methodology that enables realistic assessment of deployment feasibility under infrastructure constraints. The conceptual architecture of the proposed framework is illustrated in Figure 1.

To the best of the authors' knowledge, limited studies have simultaneously integrated GIS-based spatial feasibility filtering, cabinet-level electrical capacity constraints, structural hosting capacity derivation, and AFIR-based regulatory benchmarking within a unified optimization framework for public lighting-integrated EV charging deployment. The main contributions of this study can be summarized as follows:

- The development of a spatial–electrical coupling framework that links GIS-based pole feasibility filtering with cabinet-level electrical constraints to derive effective structural hosting capacity;

- The formulation of a grouped binary MILP model that explicitly captures cabinet-level topology and capacity limitations within public lighting infrastructure;
- The integration of AFIR-based regulatory benchmarking as a post hoc policy evaluation layer applied to optimization outputs to evaluate compliance robustness under projected EV fleet growth.

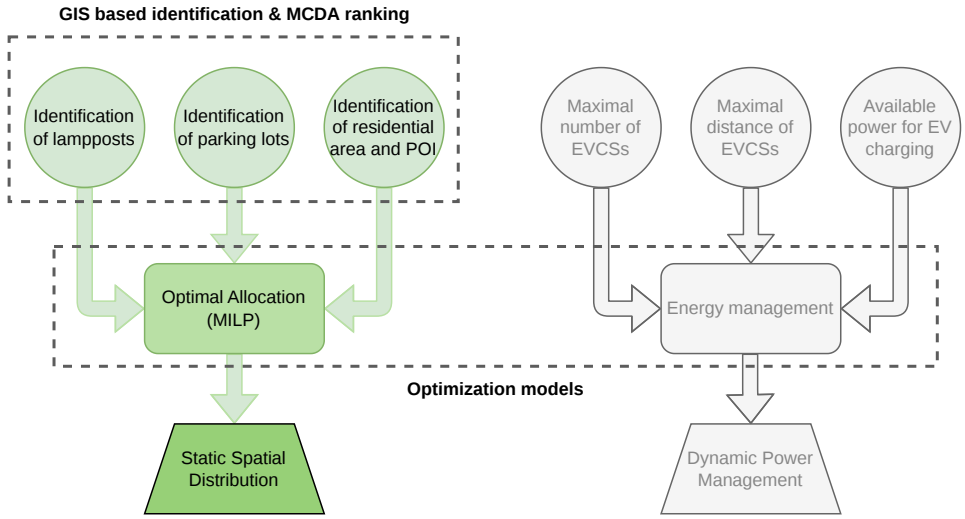


Figure 1. Conceptual architecture of the two-stage research framework: GIS-based optimal allocation of EV charging stations integrated into public lighting infrastructure (this study) and subsequent dynamic power management (future work).

The results demonstrate that while public lighting infrastructure can effectively support the initial deployment of EV charging stations, its structural hosting capacity is limited under projected EV adoption scenarios. This highlights the necessity of integrating complementary infrastructure planning strategies to ensure long-term scalability and regulatory compliance.

The Optimal Allocation process is based on GIS identification of lampposts, parking lots, and residential areas, leading to a Static Spatial Distribution. The Energy Management part considers the number, distance, and available power of EV charging stations, leading to Dynamic Power Management. The first research will be focused on Optimal Allocation. The present study focuses exclusively on the left-hand component of Figure 1, namely the optimal allocation problem under cabinet-level electrical constraints. The Dynamic Power Management component represents future work and is not addressed in this manuscript. The aim of this study is to develop an integrated GIS–MCDA–MILP framework for the optimal allocation of EV charging stations within public lighting infrastructure.

2. GIS-Based Spatial Analysis

This section presents the GIS-based methodology used to identify feasible locations and evaluate spatial demand indicators for EV charging station deployment.

2.1. Input Spatial Layers and Pre-Processing

The case study is conducted in a medium-sized city in eastern Croatia with a population of approximately 96,848 inhabitants (2021 census) and a total area of approximately 170 km^2. The city features a mixed urban parking regime comprising on-street curbside parking, perpendicular and angled parking along roadways, and off-street parking around residential buildings. The public lighting network comprises 231 cabinets and 12,863 poles in total. The location was selected for its representative urban complexity and institutional data access through cooperation with the municipal authority. It represents a data-limited

real-world context typical of medium-sized Central European cities, making it a suitable testbed for the proposed framework.

The analysis relies on multiple spatial datasets to identify feasible candidate locations and quantify demand indicators for the deployment of EV charging infrastructure.

Geographic Information Systems (GIS) were employed to identify feasible public lighting poles for EV charging integration and to quantify spatial demand indicators for ranking candidate locations. Spatial analysis was conducted using QGIS, while optimization modeling was implemented in Python 3.12.13 (Google Colaboratory) using the CBC/PuLP solver. The following vector datasets were utilized:

- Public lighting poles (points): geographic coordinates and asset identifier for each pole (decision unit).
- Parking signs (points): regulatory indicators of on-street and off-street parking availability.
- Road network (lines): street centrelines used to constrain feasible candidate areas to the roadway corridor.
- Residential demand layer:
  - Multi-apartment buildings (polygons): proxy for residential charging demand in areas with limited private charging availability.
- Public-use demand layers:
  - Public buildings (polygons/points).
  - Schools (polygons/points).
  - Sports halls and playgrounds (polygons/points).
- Public lighting cabinets (points): electrical infrastructure nodes supplying groups of lighting poles.

All spatial layers were processed in a projected coordinate reference system with metric units (HTRS96/Croatia TM, EPSG:3765), ensuring geometrically consistent buffering and Euclidean distance calculations in meters (Figure 2).

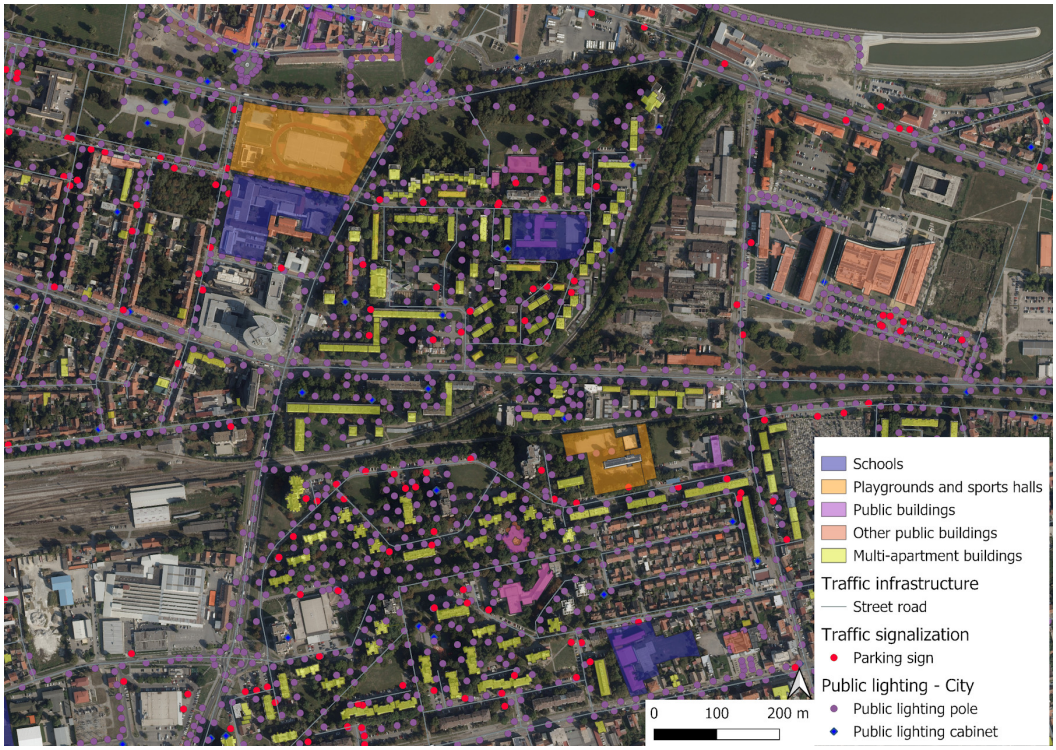


Figure 2. Study area map illustrating the primary spatial datasets: road network, parking signs, public lighting poles, and public lighting cabinets.

The spatial datasets used in this study were obtained from publicly available and institutional sources, including municipal infrastructure records and public geospatial databases. Due to data sensitivity related to critical infrastructure (the public lighting network), certain datasets are not publicly available. Aggregated or anonymized data can be provided by the authors upon reasonable request.

2.2. Feasible Candidate Area from Parking and Road Accessibility

A core feasibility requirement for pole-integrated charging is that the pole must be located where a vehicle can legally and practically park. Ideally, a georeferenced parking lot polygon layer would be used to directly identify parking areas. In the absence of such data, parking signs were used as a legal proxy for parking availability, with buffer radii selected to approximate the spatial extent that a direct parking geometry intersection would produce. Two buffer layers were created:

- Parking sign buffer B_p: a buffer of 25 m around each parking sign point, calibrated through iterative visual inspection of representative street segments to approximate the spatial influence zone of a parking sign in a typical urban context;
- Road buffer B_r: a buffer of 15 m around road lines, representing the road corridor where parking and vehicle access are physically plausible. This value was derived from the typical cross-sectional profile of urban streets in the study area. The buffer radius of 15 m from the road centreline encompasses: half the standard carriageway width (approximately 2.75 m for a minimum 5.5 m carriageway as specified in the Spatial Plan of the City of Osijek—PPUGO), a minimum perpendicular parking space depth of 5 m as prescribed by the Ordinance on Road Signs, Signalization and Equipment, a green strip of approximately 1 m, a pedestrian footpath of approximately 1.5 m, and the lateral offset of the lighting pole from the footpath edge of approximately 1 m. This yields a combined spatial envelope of approximately 11.25 m from the road centreline to the pole position, with the 15 m buffer providing a conservative margin to account for variability in street profiles and pole placement across the study area.

The initial feasible parking-accessible area was defined as the spatial intersection between the parking sign buffer and the road corridor buffer:

$$A_0 = B_p \cap B_r, \tag{1}$$

where A_0 denotes the initial parking-accessible area used as the first feasibility filter for candidate pole extraction (m^2), B_p represents the buffer polygon constructed around parking sign points with a radius of 25 m, corresponding to legally designated parking influence areas (m^2), and B_r denotes the buffer polygon constructed around road centrelines with a radius of 15 m, representing the physical road corridor where vehicle access is possible (m^2).

This operation ensures that only those areas that are both legally designated for parking (via regulatory signs) and physically located within the road corridor are retained. The intersection operation eliminates parking sign influence areas that do not spatially coincide with the roadway corridor, thereby reducing noise resulting from mapping inaccuracies or isolated regulatory sign placement.

In urban practice, parking signs may delimit longer parking stretches. Where two adjacent signs are separated by less than 50 m, their 25 m buffers overlap and continuously cover the parking stretch between them. Where the inter-sign distance exceeds this threshold, a spatial gap may appear even if parking exists continuously between signs. To account for such discontinuities between adjacent parking sign buffers along the same road corridor, gap polygons were derived as the spatial difference between the road corridor buffer and the dissolved initial accessible area:

$$G = B_r \setminus \text{dissolve}(A_0), \tag{2}$$

where G denotes the set of gap polygons representing uncovered segments within the road corridor (m^2).

Because the road buffer may generate multipart geometries, gap polygons were converted to singlepart features prior to filtering. A subset $G_s \subseteq G$ was selected based on polygon area thresholding to retain only small discontinuities that plausibly correspond to continuous parking stretches. The final accessible area is defined as:

$$A = \text{dissolve}(A_0 \cup G_s), \tag{3}$$

where A denotes the final parking-accessible area used for candidate pole extraction (m^2), and G_s represents the subset of gap polygons corresponding to selected small discontinuities (m^2).

The area threshold used for selecting G_s was set at 2000 m^2, formally defined as $G_s = \{g \in G : \text{area}(g) \leq 2000\ m^2\}$. This value was calibrated empirically through visual inspection of representative street segments. The objective was to retain only local discontinuities between adjacent parking-sign influence areas corresponding to continuous curbside parking stretches, while excluding large open spaces, intersections, and extensive road-corridor residuals not representative of continuous parking availability. An illustrative example of this procedure is shown in Figure 3, which presents a representative urban street segment and highlights the spatial relationship between curbside parking geometry and candidate pole locations, forming the basis for identifying feasible EV charging installation points.

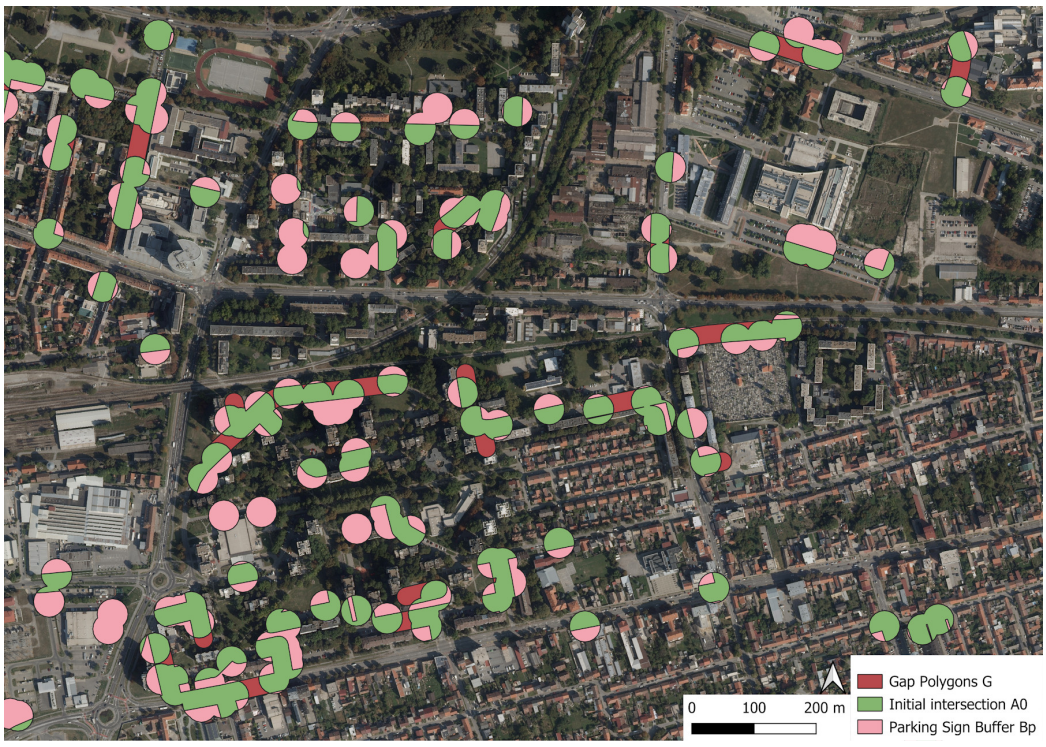


Figure 3. Example street segment illustrating (i) parking sign buffers B_p, (ii) initial intersection A_0, and (iii) derived gap polygons G. The selected subset G_s is incorporated to obtain the final accessible area A.

In GIS, the subset G_s was obtained through the following steps: (i) computing the spatial difference to derive G, (ii) converting multipart geometries to singlepart features, (iii) calculating polygon area attributes, and (iv) selecting polygons below a predefined area threshold. The threshold was calibrated based on visual inspection of representative street segments to retain only discontinuities consistent with typical parking sign spacing.

It should be noted that the buffering-based reconstruction of parking-accessible areas was adopted due to the absence of a comprehensive georeferenced parking lot polygon layer in the available dataset. When detailed parking lot polygons (representing legally designated on-street or off-street parking areas) are available, the feasibility filtering procedure can be significantly simplified. In such cases, the feasible candidate area can be defined directly as the spatial intersection between the parking lot layer and the public lighting pole layer, without the need for buffering parking signs and road centrelines. This approach provides higher spatial accuracy and reduces potential uncertainty introduced by buffer parameter selection. The buffering methodology presented here therefore represents a reproducible proxy strategy applicable in data-limited contexts, while the framework itself remains adaptable to more precise parking geometry datasets when available.

2.3. Candidate Pole Extraction

Lighting poles were treated as the decision units for subsequent ranking and optimization. The feasible candidate set was defined as all poles intersecting the final parking-accessible area A:

$$\mathcal{J} = \{j \in \mathcal{P} \ : \ j \cap A \neq \emptyset\}, \tag{4}$$

where $\mathcal{J}$ denotes the set of feasible candidate poles for EV charging station integration, $\mathcal{P}$ represents the set of all public lighting poles in the study area, and j is an index corresponding to an individual public lighting pole associated with its spatial geometry.

This operation ensures that only poles located within legally and physically accessible parking zones are retained as feasible charging candidates. The resulting layer, Poles Final Demand, contains one record for each feasible candidate pole $j \in \mathcal{J}$, including its geometry and associated attributes. The spatial distribution of the resulting candidate poles is illustrated in Figure 4.

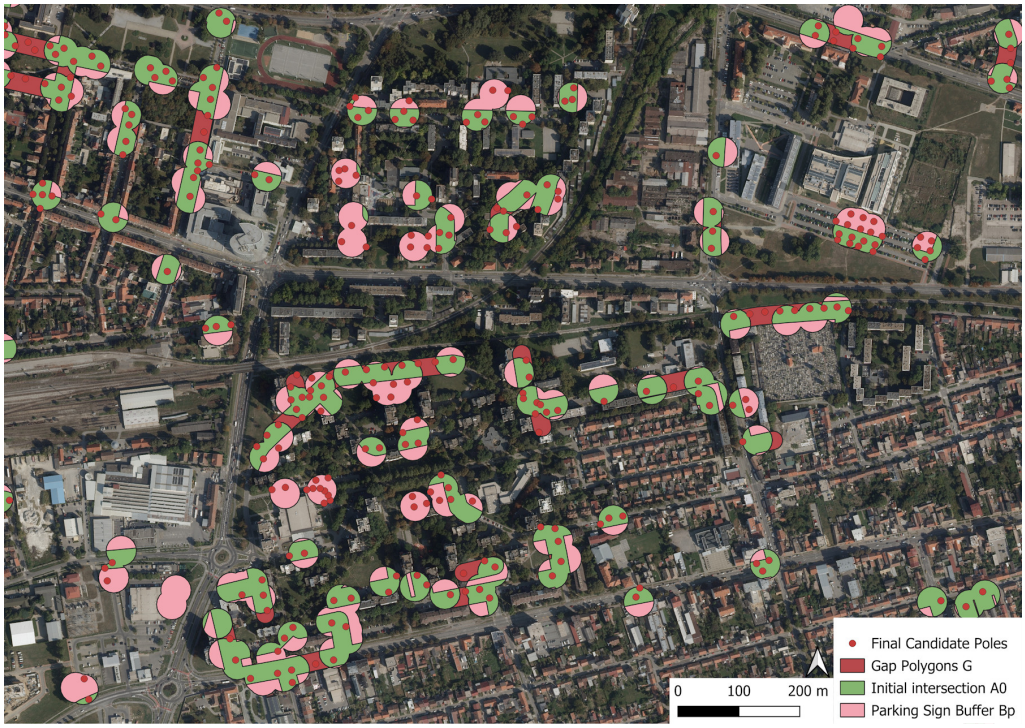


Figure 4. Spatial distribution of final candidate poles $\mathcal{J}$ retained after GIS-based feasibility filtering and forming the input set for MCDA ranking, overlaid on the final parking-accessible area A.

2.4. Demand Indicators Around Candidate Poles

For each candidate pole j, demand was quantified using a catchment radius of 300 m, representing walkable accessibility. A pole buffer was constructed as:

$$A_j = \text{buffer}(j, 300), \tag{5}$$

where A_j denotes the catchment area around candidate pole j with a radius of 300 m (m^2).

A radius of 300 m was selected to approximate walkable accessibility in urban environments [23].

2.4.1. Residential Proximity via Multi-Apartment Buildings (Count)

Multi-apartment buildings represent households with constrained home charging capability. For each candidate pole j, the residential demand indicator was defined as:

$$x_j^{(R)} = \left|\{b \in \mathcal{B}_R \ : \ b \cap A_j \neq \emptyset\}\right|, \tag{6}$$

where $x_j^{(R)}$ denotes the number of multi-apartment buildings intersecting the catchment area of pole j, $\mathcal{B}_R$ represents the set of multi-apartment buildings, and b denotes an individual building polygon.

This indicator captures the number of residential demand sources within the 300 m catchment area. Although single-family houses were available in the dataset, they were excluded from the MCDA at this stage due to their higher likelihood of private home charging availability. This represents a simplifying modelling choice rather than a universally valid assumption. In some urban contexts, single-family dwellings may also have limited practical access to home charging infrastructure, and their inclusion could be considered in future applications of the framework.

2.4.2. Proximity to Public Use Facilities (Distances)

For public facilities, distance-based indicators were preferred over counts to better reflect direct accessibility to the nearest attractor. For each candidate pole j, the following distance metrics were defined:

$$x_j^{(\text{SCH})} = \min_{k \in \mathcal{F}_{\text{SCH}}} d(j,k), \tag{7}$$

$$x_j^{(\text{PUB})} = \min_{k \in \mathcal{F}_{\text{PUB}}} d(j,k), \tag{8}$$

$$x_j^{(\text{SP})} = \min_{k \in \mathcal{F}_{\text{SP}}} d(j,k), \tag{9}$$

where $x_j^{(\text{SCH})}$, $x_j^{(\text{PUB})}$, and $x_j^{(\text{SP})}$ denote the distances from pole j to the nearest school, public building, and sports facility/playground, respectively. The function $d(j,k)$ represents the Euclidean distance between pole j and facility k, computed in meters within a projected coordinate reference system. The sets $\mathcal{F}_{\text{SCH}}$, $\mathcal{F}_{\text{PUB}}$, and $\mathcal{F}_{\text{SP}}$ denote the sets of schools, public buildings, and sports facilities/playgrounds, respectively.

These distances were computed using a nearest-hub operation based on Euclidean distance in the projected CRS (EPSG:3765). Euclidean distance is adopted as a planning-level approximation. While actual user accessibility follows the road network, straight-line distance provides a computationally efficient and spatially consistent proxy for demand indicator calculation at the candidate pole level.

Table 1 summarizes the distribution of raw demand indicators across candidate poles. The number of multi-apartment buildings within the 300 m catchment ranges from 0 to 75,

with a mean of 23.44, indicating substantial variation in residential density across the study area. The minimum value of zero reflects candidate poles whose 300 m catchment contains no multi-apartment buildings; such poles may still represent viable charging locations based on proximity to schools, public buildings, or sports facilities, as captured by the remaining MCDA indicators.

Table 1. Descriptive statistics (minimum, maximum, and mean) of demand indicators across candidate poles derived from the GIS-based spatial analysis of the study area.

Indicator	Min	Max	Mean
$x_j^{(R)}$ (count)	0	75	23.44
$x_j^{(\mathrm{SCH})}$ (m)	36.36	8988.42	537.41
$x_j^{(\mathrm{PUB})}$ (m)	17.58	2755.07	238.84
$x_j^{(\mathrm{SP})}$ (m)	6.65	4041.16	412.22

Distance-based indicators exhibit wider numerical ranges. The distance to the nearest school varies from 36.36 m to 8988.42 m, reflecting the uneven spatial distribution of educational facilities. Public buildings and sports facilities show similar variability, with maximum distances exceeding 2.7 km and 4.0 km, respectively.

These differences in scale and dispersion justify the normalization of indicators prior to aggregation within the MCDA framework.

2.5. Multi-Criteria Decision Analysis (MCDA) for Ranking

Each candidate pole j is assigned a composite suitability score derived from normalized demand indicators [23]. The criteria directions are defined as follows: the residential demand indicator $x_j^{(R)}$ is treated as a benefit criterion and is therefore maximized, while the distance-based indicators $x_j^{(\mathrm{SCH})}$, $x_j^{(\mathrm{PUB})}$, and $x_j^{(\mathrm{SP})}$ are treated as cost criteria and are therefore minimized, as shorter distances imply higher accessibility.

To enable aggregation of heterogeneous indicators (counts and distances), all criteria were normalized to the interval $[0, 1]$.

2.5.1. Normalization

A linear min–max normalization approach was adopted due to its interpretability and compatibility with weighted-sum aggregation [23,24]. For a benefit (maximizing) criterion c, the normalized score is defined as:

$$s_j^{(c)} = \frac{x_j^{(c)} - \min_{j \in \mathcal{J}} x_j^{(c)}}{\max_{j \in \mathcal{J}} x_j^{(c)} - \min_{j \in \mathcal{J}} x_j^{(c)}}, \tag{10}$$

whereas for a cost (minimizing) criterion:

$$s_j^{(c)} = \frac{\max_{j \in \mathcal{J}} x_j^{(c)} - x_j^{(c)}}{\max_{j \in \mathcal{J}} x_j^{(c)} - \min_{j \in \mathcal{J}} x_j^{(c)}}. \tag{11}$$

Here, $s_j^{(c)}$ denotes the normalized score of pole j for criterion c, and $x_j^{(c)}$ represents the corresponding raw indicator value. The index $c \in \{R, \mathrm{PUB}, \mathrm{SCH}, \mathrm{SP}\}$ identifies the considered criterion.

This transformation ensures comparability across indicators with different units and value ranges.

2.5.2. Weighted Aggregation

The overall suitability score for each candidate pole j was computed using a weighted linear aggregation:

$$\mathrm{MCDA}_j = \omega_R s_j^{(R)} + \omega_{\mathrm{PUB}} s_j^{(\mathrm{PUB})} + \omega_{\mathrm{SCH}} s_j^{(\mathrm{SCH})} + \omega_{\mathrm{SP}} s_j^{(\mathrm{SP})}, \tag{12}$$

subject to:

$$\omega_R + \omega_{\mathrm{PUB}} + \omega_{\mathrm{SCH}} + \omega_{\mathrm{SP}} = 1, \quad \omega_c \geq 0, \ \forall c \in \{R, \mathrm{PUB}, \mathrm{SCH}, \mathrm{SP}\}. \tag{13}$$

Here, MCDA_j denotes the composite suitability score of candidate pole j, and ω_c represents the weight assigned to criterion c. The weights are non-negative and sum to one to ensure interpretability of the aggregated score.

The overall suitability score is computed as a weighted sum of normalized criteria. The weight coefficients ω_c reflect the relative planning importance assigned to each criterion, with higher values indicating greater priority. The criteria structure, normalization method, and assigned weights are summarized in Table 2 above. The proposed MCDA framework provides a transparent and reproducible basis for ranking candidate locations based on heterogeneous spatial demand indicators [23,25].

Table 2. Definitions of MCDA criteria, direction, normalization method, assigned weights, and planning rationale.

Criterion	Symbol	Type	Direction	Raw Indicator	Normalization Formula	Weight	Rationale
Multi-apartment buildings (within 300 m)	$x_j^{(R)}$	Count	Max	Number of multi-apartment buildings intersecting the 300 m buffer	$\frac{x_j^{(c)} - \min_{j \in \mathcal{J}} x_j^{(c)}}{\max_{j \in \mathcal{J}} x_j^{(c)} - \min_{j \in \mathcal{J}} x_j^{(c)}}$	0.45	Represents residential demand in areas lacking private charging
Distance to nearest public building	$x_j^{(\mathrm{PUB})}$	Distance (m)	Min	Euclidean distance to nearest public building	$\frac{\max_{j \in \mathcal{J}} x_j^{(c)} - x_j^{(c)}}{\max_{j \in \mathcal{J}} x_j^{(c)} - \min_{j \in \mathcal{J}} x_j^{(c)}}$	0.25	Captures proximity to administrative and service functions
Distance to nearest school	$x_j^{(\mathrm{SCH})}$	Distance (m)	Min	Euclidean distance to nearest school	$\frac{\max_{j \in \mathcal{J}} x_j^{(c)} - x_j^{(c)}}{\max_{j \in \mathcal{J}} x_j^{(c)} - \min_{j \in \mathcal{J}} x_j^{(c)}}$	0.20	Reflects concentration of daytime activity and parking turnover
Distance to nearest sports hall or playground	$x_j^{(\mathrm{SP})}$	Distance (m)	Min	Euclidean distance to nearest sports and leisure facilities	$\frac{\max_{j \in \mathcal{J}} x_j^{(c)} - x_j^{(c)}}{\max_{j \in \mathcal{J}} x_j^{(c)} - \min_{j \in \mathcal{J}} x_j^{(c)}}$	0.10	Represents occasional and leisure-oriented demand

Weights were assigned based on planning relevance and expected charging demand intensity [23,24]. Residential multi-apartment density received the highest weight (0.45) due to limited access to private charging infrastructure in such areas. Proximity to public buildings (0.25) and schools (0.20) was assigned moderate importance to capture concentrated daytime activity patterns. Sports halls and playgrounds were assigned a lower weight (0.10), reflecting more sporadic and leisure-oriented usage profiles. A sensitivity analysis of the weighting scheme was conducted to assess the robustness of the pole ranking across alternative weight configurations. Table 3 presents five scenarios ranging from the base configuration to equal weights and single-criterion dominant schemes. Robustness is assessed using two metrics: the percentage overlap of the Top 10% candidate set relative to the base ranking, and the Spearman rank correlation coefficient ρ, which measures the monotonic agreement between two rankings on a scale from 0 (no agreement) to 1 (perfect agreement). Across all tested scenarios, the Spearman rank correlation exceeds 0.97, and the Top 10% overlap ranges from 87.7% to 100%, confirming that the ranking results are robust to plausible variations in the weighting scheme, and that the same candidate poles would be selected for installation regardless of the specific weight configuration adopted.

Table 3. MCDA sensitivity analysis: overlap of Top 10% and Top 1% candidate sets and Spearman rank correlation relative to the base weighting scheme across alternative weight configurations.

Scenario	ω_R	ω_{PUB}	ω_{SCH}	ω_{SP}	Top 10% Overlap	Spearman ρ
Base	0.45	0.25	0.20	0.10	100%	1.000
Residential dominant	0.60	0.20	0.15	0.05	95.9%	0.996
Equal weights	0.25	0.25	0.25	0.25	87.7%	0.972
Public facilities dominant	0.25	0.40	0.25	0.10	91.0%	0.970
Schools dominant	0.25	0.20	0.45	0.10	88.5%	0.975

2.5.3. Ranking and Score Distribution

Candidate poles j were ranked in descending order based on their MCDA scores. The distribution of scores was evaluated using descriptive statistics (see Table 4), including minimum, maximum, mean, median, quartiles, interquartile range, and standard deviation.

Table 4. Descriptive statistics of MCDA suitability scores for candidate poles.

Statistic	Value
Minimum	0.2270
Maximum	0.9788
Range	0.7518
Mean	0.6492
Median	0.6287
First Quartile (Q1)	0.5788
Third Quartile (Q3)	0.7196
Interquartile Range (IQR)	0.1408
Standard Deviation	0.1122
Number of Candidates (N)	1223

The observed range of suitability scores (0.2270–0.9788) indicates meaningful differentiation across candidate locations. Dispersion metrics (standard deviation = 0.1122, IQR = 0.1408) suggest moderate variability, confirming that the selected criteria and weighting scheme effectively distinguish between higher- and lower-priority poles.

The distribution of MCDA scores is illustrated in Figure 5. The histogram shows a relatively smooth distribution across the normalized interval [0, 1], without pronounced clustering at extreme values. A slight concentration is observed in the mid-to-upper range, reflecting the cumulative effect of multiple positively weighted criteria.

These ranked scores form the basis for selecting high-priority subsets (top 10%, 5%, and 1%) for subsequent spatial and infrastructure-level analysis.

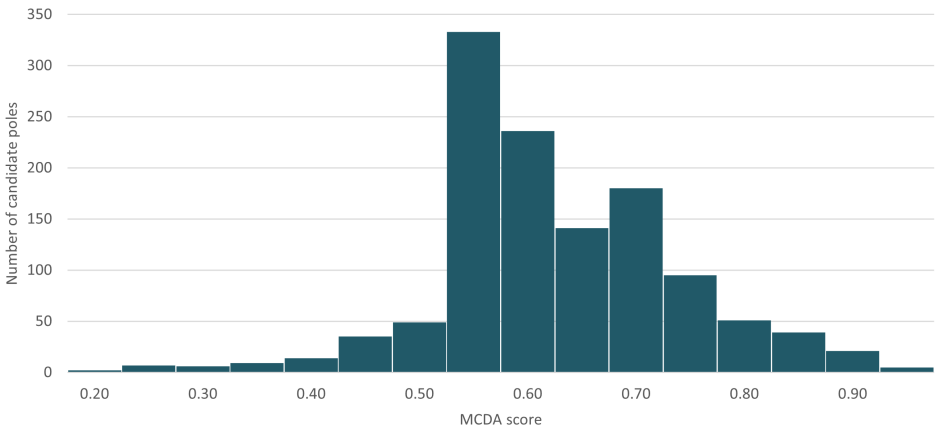


Figure 5. Histogram of MCDA scores.

2.6. Top-Percentile Candidate Sets and Hotspot Visualization

To support planning scenarios and generate interpretable shortlists, the ranked candidate set was partitioned into percentile-based subsets: top 1%, 5%, and 10%.

Let $\mathcal{J}$ denote the set of all feasible candidate poles ranked according to their MCDA scores, with cardinality $N = |\mathcal{J}|$. For a selected percentile level $p \in \{1, 5, 10\}$, the corresponding subset of top-ranked poles is defined as:

$$\mathcal{J}_{p\%} = \left\{ j \in \mathcal{J} \ : \ \text{rank}(j) \leq \left\lceil \frac{p}{100} N \right\rceil \right\}. \tag{14}$$

Here, $\text{rank}(j)$ denotes the position of pole j in descending order of MCDA score, N is the total number of feasible candidate poles, and p represents the selected percentile level.

This definition ensures consistent subset sizes across different percentile levels while preserving the ranking structure.

Heatmap Generation

Kernel density heatmaps were produced for spatial interpretation. Figure 6 presents (a) the heatmap of all candidate poles weighted by MCDA score and (b) the heatmap of the top 10% highest-ranked candidates. The resulting density surfaces reveal spatial clustering patterns consistent with high-demand areas identified through the MCDA ranking.



(**a**) (**b**)

Figure 6. Spatial distribution of EV charging demand intensity derived from MCDA-based candidate pole ranking: (**a**) full candidate set; (**b**) top 10% subset.

The heatmaps reveal pronounced spatial clustering of high-demand candidate locations. The full candidate set (Figure 6a) exhibits a broader distribution of moderate-density areas, while the top 10% subset (Figure 6b) highlights a smaller number of highly concentrated hotspots. These hotspots correspond to areas with strong combined residential demand and accessibility, confirming the effectiveness of the MCDA-based ranking in isolating priority deployment zones.

2.7. Spatial Assignment of Candidate Poles to Public Lighting Infrastructure Nodes

To establish a structured link between spatial suitability and electrical feasibility in terms of energy management, each candidate pole j was assigned to its nearest public lighting cabinet $c \in \mathcal{C}$ based on the minimum Euclidean distance:

$$c(j) = \arg\min_{c \in \mathcal{C}} d(j, c) \tag{15}$$

where $d(j, c)$ denotes the Euclidean distance computed in the projected CRS (EPSG:3765).

It should be noted that electrical cable routing data for the public lighting network were not available as a structured digital record, as the pole-to-cabinet connectivity has not been systematically documented by the network operator. Nearest Euclidean distance was therefore adopted as the most reproducible and spatially consistent proxy available under these data conditions. This simplifying assumption may introduce assignment errors where the electrically connected cabinet differs from the geographically nearest one, potentially affecting cabinet-level grouping constraints and hosting capacity calculations. The framework can be directly improved when actual electrical topology data become available, as the optimization model structure requires only a reassignment of poles to cabinets without any structural modification.

This mapping enables aggregation at the cabinet level. The subset of poles assigned to cabinet c is defined as $\mathcal{J}_c = \{j \in \mathcal{J} : c(j) = c\}$, with cardinality $n_c = |\mathcal{J}_c|$.

$$\overline{\mathrm{MCDA}}_c = \frac{1}{n_c} \sum_{j \in \mathcal{J}_c} \mathrm{MCDA}_j, \tag{16}$$

$$\mathrm{MCDA}_c^{\max} = \max_{j \in \mathcal{J}_c} \mathrm{MCDA}_j \tag{17}$$

The cabinet-level aggregation reveals how high-ranking candidate poles are distributed across the existing electrical infrastructure. Cabinets with higher values of n_c indicate spatial clustering of demand, while elevated values of $\overline{\mathrm{MCDA}}_c$ and $\mathrm{MCDA}_c^{\max}$ highlight infrastructure nodes associated with particularly strong suitability scores.

Additionally, the Top 10% candidate subset $\mathcal{J}_{10\%}$ was joined with cabinet identifiers and aggregated at the cabinet level, yielding the number of top-ranked poles per cabinet. In the study area, the Top 10% candidates were concentrated within a limited subset of cabinets (e.g., 23 cabinets), indicating pronounced spatial clustering of high-priority locations.

Table 5 summarizes cabinet-level aggregation restricted to the Top 10% of candidate poles ranked by MCDA suitability. Out of 160 public lighting cabinets in the study area, 23 host at least one top-ranked pole, indicating a pronounced spatial concentration of high-priority locations.

Table 5. Cabinet-level aggregation statistics for the Top 10% highest-ranked candidate poles, identifying infrastructure nodes with the highest concentration of priority deployment opportunities.

Cabinet ID	Count	Max	Mean
231	11	0.9788	0.9292
233	15	0.9765	0.9014
139	2	0.9674	0.9620
106	4	0.9391	0.8807
219	8	0.9252	0.8894
104	4	0.9224	0.8435
235	7	0.9133	0.8586
210	5	0.9015	0.8536
298	14	0.8976	0.8276
52	7	0.8940	0.8501
234	7	0.8894	0.8436
84	5	0.8836	0.8741
218	4	0.8733	0.8643
130	1	0.8577	0.8577
28	2	0.8569	0.8301
300	7	0.8475	0.8264
80	1	0.8425	0.8425
41	4	0.8250	0.8149
43	4	0.8246	0.8164

Table 5. *Cont.*

Cabinet ID	Count	Max	Mean
77	1	0.8146	0.8146
242	7	0.8086	0.8045
42	1	0.7973	0.7973
63	1	0.7968	0.7968

Several cabinets accommodate multiple high-ranking poles (e.g., cabinets 233 and 298), suggesting localized clustering of demand within specific infrastructure nodes. At the same time, elevated mean suitability scores across many cabinets indicate consistently strong spatial suitability within these clusters, rather than isolated high-scoring outliers.

These results highlight that high-priority candidate locations are not uniformly distributed but instead concentrate within a limited subset of cabinets. This spatial pattern supports the introduction of cabinet-level grouping constraints in the subsequent optimization model, enabling infrastructure-aware allocation strategies.

The observed concentration further reflects underlying urban morphology, where dense residential areas and key public facilities co-locate spatially. This consistency reinforces the validity of the selected MCDA criteria and confirms that the ranking procedure captures meaningful demand patterns rather than random spatial variation, as illustrated in Figure 7.

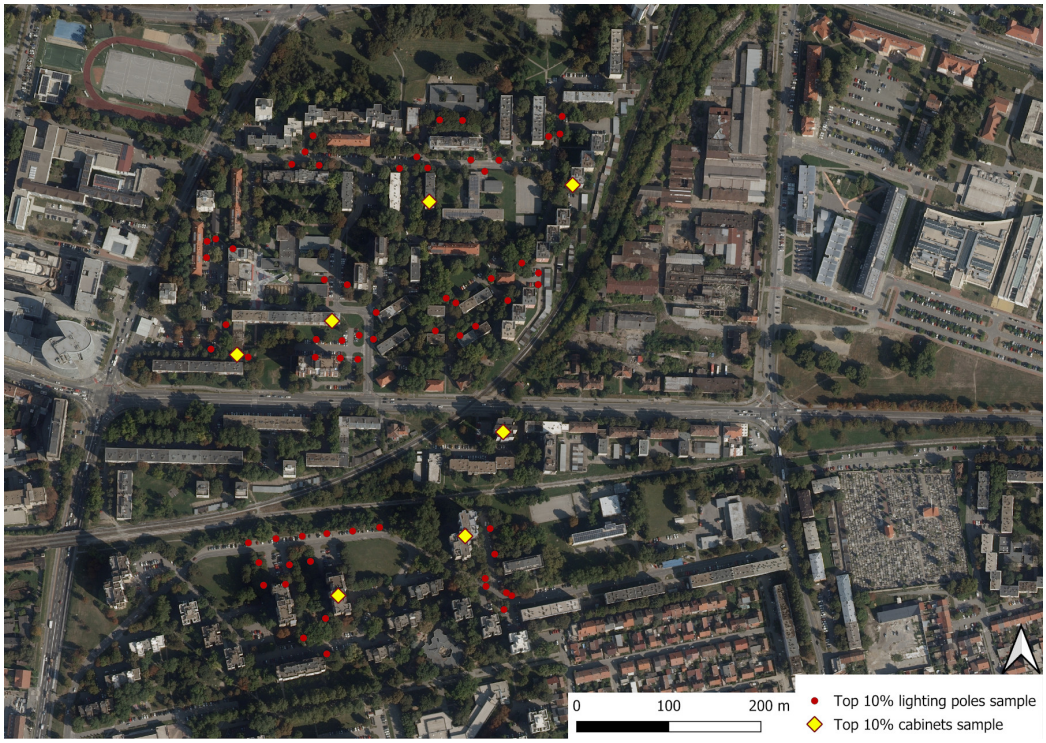


Figure 7. Public lighting cabinets symbolized by the number of Top 10% candidate poles assigned to each cabinet, illustrating the spatial concentration of high-priority deployment opportunities within a limited subset of cabinet service areas.

The concentration of high-ranking poles within a limited number of cabinets indicates that unconstrained selection may lead to excessive allocation within individual feeder segments. To prevent over-concentration and ensure spatially balanced deployment, a cabinet-level grouping constraint is introduced in the subsequent optimization model:

$$\sum_{j \in \mathcal{J}_k} x_j \leq M_k, \quad \forall k \in \mathcal{C} \tag{18}$$

Here, $x_j \in \{0,1\}$ is a binary decision variable indicating whether candidate pole j is selected for EV charging station installation. The set $\mathcal{J}_k = \{j \in \mathcal{J} : c(j) = k\}$ represents candidate poles assigned to cabinet k, and M_k is a planning parameter defining the maximum allowable number of charging stations connected to cabinet k. This constraint directly links spatial suitability analysis with infrastructure capacity considerations, enabling the optimization model to account for both demand intensity and network limitations.

2.8. Practical Note on Completeness and Contingency

Because parking geometry was reconstructed from regulatory parking sign points and road corridors, rather than derived from complete parking polygon inventories, the resulting candidate set $\mathcal{J}$ may not capture all technically feasible locations. While this approach ensures transparency and reproducibility, it may underrepresent certain parking configurations not fully reflected in sign-based mapping.

To mitigate this limitation, the subsequent optimization stage incorporates contingency mechanisms designed to preserve solution robustness:

- Allowing a controlled fraction of selections beyond strict top-percentile subsets (e.g., extending beyond the top decile);
- Applying cabinet-level flexibility rules that retain capacity for additional candidate poles within the same service area during detailed feasibility assessment.

These provisions enhance robustness against potential spatial omissions while maintaining a transparent and GIS-driven candidate generation framework.

Building on the observed clustering of high-priority candidate poles within specific public lighting cabinets, the following section formulates a mixed-integer linear programming (MILP) model. The MCDA suitability scores derived in the preceding section serve directly as objective function coefficients in the MILP formulation, ensuring that the constrained selection stage maximizes aggregate spatial suitability while respecting cabinet-level electrical capacity limits. The model explicitly incorporates cabinet-level grouping constraints to ensure both technical feasibility and spatially balanced deployment of EV charging infrastructure.

3. Optimization Approach

3.1. Problem Definition

The planning and deployment of public EV charging infrastructure is a critical component of sustainable urban mobility and electric grid integration. As the number of EVs continues to grow globally, the strategic placement of charging stations must balance accessibility, cost-effectiveness, and grid reliability [5,16]. This problem has been widely studied in the literature, where siting and sizing of charging infrastructure are formulated as optimization problems that seek to maximize user coverage, minimize costs, and account for demand and grid constraints [2,9,11].

Various modelling approaches have been proposed for EV charging infrastructure planning, including mathematical programming, metaheuristic optimization, and multi-objective decision-making frameworks [2,9,15]. Mixed-integer formulations are particularly common when binary location decisions and capacity constraints must be simultaneously addressed [11,26].

In this work, the allocation problem is defined as the selection of a subset of feasible public lighting poles for the installation of slow AC charging units (3.68 kW). The candidate poles are pre-identified using GIS-based spatial filtering and multi-criteria decision analysis

(MCDA), resulting in a ranked set of technically and spatially feasible locations. The optimization stage determines the optimal subset of these candidates for deployment.

The optimization model must satisfy three principal planning requirements:

1. Deployment phase constraint—Urban charging infrastructure is typically implemented in phased rollouts aligned with municipal budget cycles and mobility strategies [27]. Rather than assuming full scale deployment at once, the model introduces a deployment parameter representing the maximum number of charging units installed within a given planning phase. For example, pilot deployment phases may include 10–15 units, while intermediate and large-scale scenarios may consider 60 or more installations.
2. Cabinet-level power constraints—Each public lighting pole is electrically connected to a cabinet with finite rated capacity. Charging units integrated into lighting infrastructure must not exceed available electrical capacity to ensure distribution network reliability and prevent local overloading. In this study, the allowable charging capacity per cabinet is conservatively limited to 80% of its rated capacity to preserve operational safety margins and accommodate additional smart-city loads.
3. Technical feasibility conditions—Installation is restricted to poles that satisfy electrical, physical and regulatory feasibility requirements including feeder compatibility and compliance with local safety regulations. Technical feasibility is pre-screened during the GIS filtering stage; therefore, the optimization operates only on poles that satisfy minimum electrical and spatial criteria.

3.2. Selection of Optimization Framework

The optimal placement of EV charging infrastructure has been addressed using a wide range of optimization methodologies, including mixed-integer linear programming (MILP), nonlinear and quadratic programming, and metaheuristic algorithms such as Genetic Algorithms (GA) and Particle Swarm Optimization (PSO), as well as clustering-based approaches [6,9,15]. The choice of modelling framework depends on the structural characteristics of the decision problem, including the type of decision variables, the nature of constraints, and computational tractability.

In the present study, the allocation problem is characterized by binary installation decisions, linear objective aggregation, and linear infrastructure constraints. The suitability score associated with each candidate pole is predefined, and no nonlinear interaction terms or continuous power flow variables are required at this stage. Consequently, the problem naturally conforms to a 0–1 linear programming structure.

Mixed-Integer Linear Programming (MILP) is selected as the primary optimization framework for several reasons. First, MILP guarantees global optimality for problems with linear objectives and constraints, provided that computational limits are not exceeded [26,28]. Given that the number of candidate poles in the study area is on the order of approximately 10^3, modern MILP solvers can efficiently compute exact solutions without the need for approximation.

Second, heuristic and metaheuristic approaches such as GA, PSO, and Simulated Annealing are typically employed in highly nonlinear or large-scale combinatorial problems where exact methods become computationally prohibitive [9,17]. While such methods may offer flexibility, they do not guarantee global optimality and often require parameter tuning and repeated runs to ensure stability. Since the present problem is structurally linear and of moderate size, the use of heuristic approaches would introduce unnecessary approximation error.

Third, quadratic programming models are sometimes adopted when spatial interaction effects or distance-based penalties are explicitly modelled [29,30]. However, in the

proposed formulation, spatial suitability is already embedded within the MCDA score, and no quadratic interaction terms between candidate locations are required. Therefore, a linear formulation is sufficient and preferable due to its interpretability and computational robustness.

For these reasons, the allocation problem is formulated as a MILP model. This choice ensures mathematical transparency, reproducibility, and exact solution quality while remaining computationally efficient for urban-scale applications.

3.3. Mathematical Formulation

Following the problem definition and the selection of Mixed-Integer Linear Programming (MILP) as the optimization framework, the allocation of charging units to public lighting poles is formulated as a 0-1 mixed-integer linear programming (MILP) problem. Similar binary location-allocation formulations have been widely applied in EV charging infrastructure planning [15,16,26].

Let $\mathcal{J}$ denote the set of feasible candidate poles for EV charging station integration, as defined in the previous section:

$$\mathcal{J} = \{j \in \mathcal{P} : j \cap A \neq \emptyset\} \tag{19}$$

Each pole represents a potential installation point for a 3.68 kW AC charging unit. The set of public lighting cabinets supplying electrical power to subsets of poles is represented by $\mathcal{C}$. Each candidate pole is electrically assigned to exactly one cabinet. Accordingly, let $\mathcal{J}_k = \{j \in \mathcal{J} : c(j) = k\}$ represent the subset of feasible candidate poles electrically assigned to cabinet $k \in \mathcal{C}$.

This grouping structure enables the incorporation of cabinet-level electrical constraints, which are commonly considered in grid-aware charging allocation models [9,11].

For each candidate pole $j \in \mathcal{J}$, a binary decision variable is defined:

$$x_j = \begin{cases} 1, & \text{if a charging unit is installed at pole } j, \\ 0, & \text{otherwise.} \end{cases} \tag{20}$$

Binary decision modelling is standard in charging station siting problems where installation is a discrete choice [16,26].

The objective of the model is to maximize the aggregated spatial suitability of the selected poles. Each candidate pole is associated with a composite suitability score MCDA_j, derived from normalized demand indicators as described in the section above.

The objective function is defined as:

$$\max \sum_{j \in \mathcal{J}} \mathrm{MCDA}_j \, x_j \tag{21}$$

This linear aggregation prioritizes installation at poles with higher composite demand scores. Similar weighted-sum objective structures are widely used in charging infrastructure location problems where demand proxies are precomputed [5,10,13,16].

Urban EV infrastructure is typically implemented in stages reflecting budget availability and municipal planning cycles [3]. To model this phased deployment, the total number of installed charging units is limited by a deployment parameter N_{phase}, representing the maximum number of installations allowed within a given planning phase. The constraint is formulated as:

$$\sum_{j \in \mathcal{J}} x_j \leq N_{\text{phase}}, \tag{22}$$

where N_{phase} denotes the maximum number of charging units installed within the considered deployment phase. This formulation enables scenario-based analysis of pilot, intermediate, and large-scale rollouts without altering the structural model.

Each candidate pole $j \in \mathcal{J}$ is electrically connected to a public lighting cabinet $k \in \mathcal{C}$, where $\mathcal{J}_k = \{j \in \mathcal{J} : c(j) = k\}$ represents the subset of feasible candidate poles electrically assigned to cabinet k. This grouping structure enables the incorporation of cabinet-level electrical constraints, which are commonly considered in grid-aware charging allocation models [9,11].

Each cabinet has a rated electrical capacity P_k^{rated}. Since charging units introduce additional load to the lighting infrastructure, the total installed charging power connected to a cabinet must remain within its allowable capacity to ensure safe operation of the distribution system. In distribution planning practice, sustained loading close to rated capacity is generally avoided in order to preserve thermal margins, maintain voltage stability, and account for load variability. Therefore, a conservative utilization factor of $\alpha = 0.8$ is applied, limiting the allowable charging load to 80% of the rated cabinet capacity. This margin preserves operational reliability while accommodating potential future smart-city loads. In this study, each integrated AC charging unit is assumed to have a nominal power of $P_{\text{charger}} = 3.68$ kW, corresponding to single-phase slow charging typically used for residential and destination charging. The selected charging power reflects typical low-voltage single-phase charging compatible with public lighting circuits without requiring major grid reinforcement. The maximum number of chargers that can be connected to cabinet k is therefore defined as:

$$U_k = \left\lfloor \frac{\alpha \cdot P_k^{\text{rated}}}{P_{\text{charger}}} \right\rfloor, \tag{23}$$

where P_k^{rated} denotes the rated power capacity of cabinet k (kW), P_{charger} is the nominal power of one single-phase AC charging unit (kW), α is the conservative utilization factor, and U_k is the maximum number of chargers allowed at cabinet k.

The selection of $\alpha = 0.8$ is consistent with conventional low-voltage distribution planning practice, where continuous loading is typically limited to 80–85% of rated capacity to preserve thermal margins and mitigate accelerated insulation aging. Typical operational loading limits in low-voltage distribution systems range between 70% and 85% of rated capacity depending on asset type and thermal constraints [31].

The parameter U_k is computed prior to optimization from cabinet data and treated as a fixed integer input to the optimization model. The cabinet-level constraint is then expressed as:

$$\sum_{j \in \mathcal{J}_k} x_j \leq U_k, \quad \forall k \in \mathcal{C} \tag{24}$$

This grouped capacity constraint ensures that the installed charging load at each cabinet remains within infrastructure limits.

Finally, the binary nature of installation decisions is enforced through:

$$x_j \in \{0, 1\}, \quad \forall j \in \mathcal{J} \tag{25}$$

The resulting formulation corresponds to a 0-1 knapsack-type selection problem with grouped capacity constraints at cabinet level. The model combines a cardinality constraint (deployment phase limit) with multiple grouped knapsack constraints representing electrical cabinet capacities.

The model contains $|\mathcal{J}|$ binary decision variables and $|\mathcal{C}| + 1$ linear constraints. In the present case study, this corresponds to 1223 binary variables and 161 linear constraints,

resulting in a moderate-scale MILP that can be solved to proven global optimality using modern solvers.

The model outputs:

- The optimal subset of poles selected for installation;
- The distribution of charging units across cabinets;
- The total installed charging capacity per deployment phase.

Time-dependent charging demand and operational load variability are not considered in this static allocation model.

3.4. Infrastructure-Based Capacity Derivation

The mathematical formulation introduced above requires cabinet-level rated electrical capacity as an input parameter. This section describes how infrastructure constraints are derived from real distribution data and translated into optimization parameters.

Public lighting poles in the study are supplied by a set of low-voltage public lighting cabinets. Each cabinet $k \in \mathcal{C}$ is characterized by a rated electrical capacity P_k^{rated} [kW], obtained from municipal or utility infrastructure records.

Since charging units introduce additional load to the lighting system, the available capacity for EV charging must be determined conservatively. In accordance with standard distribution system planning practice, sustained operation close to rated capacity is avoided in order to preserve thermal margins, ensure voltage stability and account for demand variability [31]. Therefore, only a fraction $\alpha = 0.8$ of rated capacity is considered available for charging integration.

The allowable charging capacity per cabinet is therefore computed as:

$$P_k^{\text{avail}} = \alpha \cdot P_k^{\text{rated}}, \tag{26}$$

where P_k^{avail} denotes the available power capacity for EV charging [kW].

Given the nominal power of one charging unit $P_{\text{charger}} = 3.68$ kW, the parameter U_k introduced above is computed from infrastructure data as follows:

$$U_k = \left\lfloor \frac{P_k^{\text{avail}}}{P_{\text{charger}}} \right\rfloor \tag{27}$$

Because charging units are discrete devices with fixed nominal power, fractional values of the capacity ratio are rounded to the nearest lower integer to ensure feasibility within cabinet limits.

The parameter U_k is calculated prior to optimization and treated as a fixed integer input. This ensures that cabinet-level infrastructure constraints are explicitly respected within the MILP formulation.

This infrastructure-based derivation enables realistic modelling of electrical feasibility and prevents over-allocation of charging units at cabinets with limited residual capacity.

3.5. Policy-Based Benchmarking Framework

Beyond technical feasibility, urban EV charging infrastructure planning must also align with European Union regulatory requirements governing minimum public charging deployment. Regulation (EU) 2023/1804 on the deployment of alternative fuels infrastructure (AFIR) establishes minimum public charging power requirements proportional to the size of the national EV fleet [3].

For light-duty vehicles, Member States must ensure that publicly accessible charging infrastructure provides at least:

- 1.3 kW per battery electric vehicle (BEV), and;

- 0.8 kW per plug-in hybrid electric vehicle (PHEV).

To contextualize the model results, the required minimum public charging power is computed as:

$$P_{\text{AFIR}} = 1.3 \cdot N_{\text{BEV}} + 0.8 \cdot N_{\text{PHEV}}, \tag{28}$$

where N_{BEV} denotes the number of registered battery electric vehicles, N_{PHEV} the number of registered plug-in hybrid vehicles, and P_{AFIR} the minimum required public charging power [kW].

For city-level benchmarking, the national fleet-based requirement is proportionally scaled to the study area based on the estimated local EV fleet size.

Since the present study focuses exclusively on slow AC charging integrated into public lighting infrastructure, only the slow-charging share of the total AFIR requirement is considered for benchmarking. Slow and destination charging is particularly well-suited to urban residential areas, where vehicles remain parked for extended periods and fast charging primarily serves interurban corridors [4,32]. A conservative slow-charging share of $\beta = 0.7$ is therefore adopted for benchmarking purposes [32,33].

Accordingly, the slow-charging target power and total installed charging power are defined as:

$$P_{\text{slow,target}} = \beta \cdot P_{\text{req}}^{\text{AFIR}}, \tag{29}$$

$$P_{\text{installed}} = P_{\text{charger}} \cdot \sum_{j \in \mathcal{J}} x_j, \tag{30}$$

where $P_{\text{slow,target}}$ denotes the slow-charging power target used for benchmarking [kW], β is the proportion of total charging demand attributed to slow charging, and $P_{\text{installed}}$ is the total installed charging power [kW].

The total installed charging power resulting from the optimization model is then compared against this benchmark to evaluate the contribution of public lighting-integrated chargers to overall regulatory compliance:

$$\gamma = \frac{P_{\text{installed}}}{P_{\text{slow,target}}}, \tag{31}$$

where γ denotes the proportion of the slow AFIR charging power target satisfied. A value of $\gamma \geq 1$ indicates that the optimized lighting-integrated deployment fully satisfies the slow-charging share of the AFIR requirement.

This benchmarking approach allows assessment of:

- The share of AFIR slow-charging demand covered by lighting integration;
- The extent to which phased deployment scenarios support regulatory targets;
- The realistic contribution of existing infrastructure repurposing.

Importantly, AFIR is not implemented as a hard constraint in the optimization model, but rather as an external policy reference for interpreting results.

3.6. Computational Performance

The MILP model was implemented in Python and executed within the Google Collaboratory cloud computing environment. The optimization problem was formulated using the PuLP linear programming modeling package in Python and solved using the open-source CBC (Coin-or Branch and Cut) MILP solver.

All preprocessing and spatial data handling were performed using standard scientific Python libraries, including pandas (data management), numpy (numerical computation), geopandas (spatial data processing), and shapely (geometric operations).

The optimization model contains 1223 binary decision variables and 161 linear constraints (160 cabinet-level capacity constraints and one deployment constraint). For all examined deployment scenarios, the solver terminated with proven global optimality (MIPGap = 0%). Preliminary testing indicates solution times below one second per scenario, confirming computational tractability for urban-scale candidate sets. All experiments were repeated across multiple solver seeds to confirm solution stability.

All numerical results reported in Sections 4.2–4.4 were reproduced in an independent execution of the Google Colab environment using the same input dataset and model formulation. The theoretical hosting capacity (409 chargers), structural hosting capacity (368 chargers), phased deployment outcomes (12, 61, and 122 chargers), and AFIR benchmarking indicators were fully consistent across repeated runs, confirming computational reproducibility of the proposed MILP framework.

3.7. Comparison of MILP Allocation and Top-N Ranked Selection

To demonstrate the added value of the MILP formulation over a simple top-N ranked selection, a direct comparison was conducted for each phased deployment scenario. The naïve top-N approach selects the N highest-ranked poles by MCDA score without accounting for cabinet-level capacity constraints, while the MILP model enforces these constraints explicitly. Table 6 summarizes the results.

Table 6. Comparison of MILP optimization against naïve top-N ranked selection across phased deployment scenarios, showing cabinet constraint violations, pole overlap, and aggregated MCDA score difference.

Phase	Cabinet Violations (Top-N)	Pole Overlap	MCDA Score Difference
Phase 1 ($N = 12$)	2	75.0%	0.52%
Phase 2 ($N = 61$)	8	44.3%	5.73%
Phase 3 ($N = 122$)	15	36.1%	7.86%

The results demonstrate that naïve top-N selection produces infeasible solutions in all three deployment scenarios, violating cabinet-level capacity constraints at 2, 8, and 15 cabinets respectively. The MILP model resolves these violations while retaining the highest achievable aggregate suitability score under the imposed constraints. As deployment scale increases, the divergence between the two approaches grows substantially, confirming that cabinet-level constraints become increasingly binding and that the MILP formulation provides material added value beyond ranked shortlist selection.

4. Results and Discussion

This section presents the results of the proposed GIS-based MILP allocation model applied to the study area. Building upon the spatial filtering and MCDA ranking framework developed in the previous sections, the optimization model is evaluated under phased deployment scenarios, infrastructure capacity constraints, and policy benchmarking conditions.

The results are structured in four stages. First, a dataset overview is provided to summarize the structural characteristics of the candidate set and the electrical infrastructure. Second, the base scenario optimization results are presented for phased deployment cases. Third, infrastructure-based scenario analysis is conducted to evaluate the hosting capacity limits of the public lighting system. Finally, the contribution of lighting-integrated charging deployment to AFIR compliance is assessed through a policy benchmarking framework.

The analysis aims to quantify:

- The effective hosting capacity of public lighting infrastructure;

- The spatial distribution of optimal charging locations;
- The extent to which phased deployments support regulatory requirements;
- The robustness of infrastructure reuse under projected EV growth.

4.1. Dataset Overview

4.1.1. Candidate Pole Set

Following GIS-based spatial filtering and MCDA ranking, a total of 1223 feasible candidate poles were identified for potential EV charging integration. These poles satisfy both parking-accessibility constraints and proximity-based demand criteria.

Each candidate pole is electrically connected to one of 160 public lighting cabinets, which represent the electrical supply nodes of the low-voltage lighting network.

The candidate poles were previously ranked according to their composite MCDA suitability scores, forming the input set for the optimization stage.

4.1.2. Cabinet Level Electrical Capacity

Electrical feasibility is governed by cabinet-level rated capacity and the conservative utilization factor $\alpha = 0.8$. Based on infrastructure records and the nominal charging power of 3.68 kW per unit, the maximum number of chargers permitted at each cabinet U_k was computed.

The distribution of cabinet capacities is summarized in Table 7.

Table 7. The distribution of cabinet capacities (all charging units: 3.68 kW single-phase slow AC).

Maximum Chargers per Cabinet (U_k)	Number of Cabinets
0	3
2	115
3	16
4	14
5	4
6	4
7	1
8	3

The majority of cabinets (115 out of 160) can accommodate up to two charging units under the conservative loading assumption. A smaller subset supports higher capacities (3–8 units), reflecting variations in rated cabinet power across the network.

4.1.3. Theoretical and Structural Hosting Capacity

Two distinct capacity limits can be formally defined:

$$N_{\text{theo}} = \sum_{k} U_k, \tag{32}$$

$$N_{\text{struct}} = \sum_{k \in \mathcal{C}} \min(U_k, |\mathcal{J}_k|), \tag{33}$$

where N_{theo} denotes the theoretical electrical capacity, which represents the total number of chargers that could be installed if every cabinet were fully saturated, and N_{struct} denotes the structural capacity (pole-limited), which represents the real upper bound of lighting-integrated charging deployment under current spatial constraints. $|\mathcal{J}_k|$ denotes the number of feasible candidate poles connected to cabinet k. For the present case study, substituting the infrastructure data yields $N_{\text{theo}} = 409$ and $N_{\text{struct}} = 368$ chargers.

By construction, the structural hosting capacity satisfies $N_{\text{struct}} \leq N_{\text{theo}}$, where equality holds only if each cabinet possesses a sufficient number of spatially feasible poles to

fully utilize its rated electrical capacity. Structural hosting capacity therefore represents a spatially constrained upper bound on realizable electrical hosting potential.

The structural capacity reflects the effective upper bound of deployment under current spatial constraints.

Cabinet-level analysis reveals that the shortfall between theoretical and structural hosting capacity is not uniformly distributed across the network but is spatially concentrated within specific feeder segments and cabinet service areas. Out of 231 cabinets in the study area, only 29 host at least one Top-10% candidate pole, while 3 cabinets have zero electrical hosting capacity. Furthermore, the two highest-ranked cabinets alone concentrate 29 Top-10% candidate poles (15 and 14 respectively), confirming strong spatial clustering of practical deployment opportunities. Many cabinets possess sufficient rated electrical power but are associated with a limited number of feasible curbside poles due to parking geometry constraints, urban morphology, and demand distribution. In practice, electrical infrastructure availability alone therefore overestimates deployable EV charging capacity as illustrated in Figure 7.

Structural saturation refers to the condition in which all spatially feasible candidate poles permitted by cabinet-level electrical capacity constraints have been selected. This differs from theoretical electrical saturation, which assumes sufficient feasible poles at every cabinet regardless of spatial constraints. The implications of structural saturation in terms of maximum installable charging power are evaluated in the following section.

4.2. Base Scenario Optimization Results

4.2.1. Phased Deployment Scenarios

To reflect realistic municipal rollout strategies, the optimization model was evaluated under three phased deployment scenarios:

- Phase 1 (Pilot deployment): $N_{\text{phase}} = 12$ chargers;
- Phase 2 (Intermediate expansion): $N_{\text{phase}} = 61$ chargers;
- Phase 3 (Large-scale rollout): $N_{\text{phase}} = 122$ chargers.

These deployment levels were derived directly from the MCDA ranking results, corresponding to the top 1%, 5%, and 10% of the 1223 ranked candidate poles respectively. This percentile-based parameterisation ensures a transparent and reproducible link between the spatial ranking stage and the optimization input. The selected thresholds also provide meaningful policy reference points: Phase 1 and Phase 2 fall below the AFIR slow-charging benchmark ($\gamma = 0.11$ and $\gamma = 0.57$ respectively), while Phase 3 exceeds it ($\gamma = 1.14$), demonstrating that when benchmarked against AFIR requirements post hoc, the top 10% deployment threshold represents the minimum scale associated with regulatory compliance under current EV penetration levels.

These values represent progressively scaled implementation levels while preserving identical spatial and electrical constraints. The MILP model was solved independently for each deployment level, maximizing aggregated MCDA suitability subject to cabinet constraints.

4.2.2. Optimization Outcomes

The results of the three deployment scenarios are summarized in the table below (Table 8).

Installed charging power was computed as:

$$P_{\text{installed}} = N_{\text{phase}} \cdot P_{\text{charger}}, \tag{34}$$

where N_{phase} denotes the number of installed chargers per deployment scenario phase.

Table 8 shows that in all scenarios, the number of installed chargers exactly equals the predefined deployment limit. Consequently, installed power scales linearly with the rollout size. The practical interpretation of each deployment phase and its policy implications are discussed in detail in the preceding section and further elaborated in Section 4.4.

Table 8. Optimization results under phased deployment scenarios, illustrating the linear scaling of installed charging power with deployment level under non-binding cabinet constraints.

Scenario	Chargers Installed	Installed Power [kW]
Phase 1	12	44.16
Phase 2	61	224.48
Phase 3	122	448.96

4.2.3. Binding Constraint Analysis

For all three scenarios, the number of selected poles satisfied:

$$\sum_{j \in \mathcal{J}} x_j = N_{\text{phase}} \tag{35}$$

This indicates that the deployment constraint is binding, while cabinet-level capacity constraint remains non-binding within the examined deployment range. Formally:

$$N_{\text{phase}} < N_{\text{struct}}, \tag{36}$$

where $N_{\text{struct}} = 368$ chargers in the present case study. Therefore, infrastructure capacity does not restrict allocation under base rollout scenarios. Cabinet constraints are inactive in base scenarios but become binding at structural saturation. This finding implies that, under current assumptions, deployment scale is determined by policy or budgetary constraints rather than by electrical hosting capacity.

4.2.4. Spatial Allocation Pattern

In each scenario, the optimization selects the highest-ranked poles according to MCDA suitability, while respecting cabinet grouping constraints (see Figure 7 for the spatial distribution of top-ranked candidate poles across the public lighting cabinet network). The resulting spatial pattern exhibits several consistent characteristics:

- High-priority poles are concentrated within a limited subset of cabinets, reflecting spatial clustering identified in the MCDA ranking stage;
- Cabinet-level capacity constraints prevent excessive concentration of chargers within individual electrical nodes;
- Selected poles are predominantly located in dense multi-apartment residential areas and in proximity to public facilities.

In Phase 3, although 122 chargers are installed, this corresponds to only 33% of the structural hosting capacity.

Thus, approximately two-thirds of the available infrastructure headroom remains unused even under the large-scale rollout scenario.

4.2.5. Interpretation of Base Scenario Results

The base scenario analysis yields three key insights:

- Public lighting infrastructure possesses substantial unused hosting capacity. Even the largest deployment phase utilizes only one-third of the structural limit.
- Phased rollout scenarios remain far below electrical saturation. Cabinet capacity constraints do not become active within the considered deployment levels.

- Electrical feasibility does not limit near-term expansion. Under current EV penetration levels, infrastructure reuse through lighting integration is viable at the planning level without grid reinforcement.

These results establish a clear baseline for subsequent infrastructure stress testing and policy benchmarking.

4.3. Scenario Analysis

4.3.1. Structural Saturation and Capacity Limits

While the phased deployment scenarios examined in previous section reflect realistic municipal rollout levels, they do not explore the full technical potential of the lighting infrastructure. To assess the ultimate hosting capacity of the system, a structural saturation scenario was evaluated.

In this scenario, the deployment parameter is relaxed such that:

$$N_{\text{phase}} \geq N_{\text{struct}} \tag{37}$$

The structural hosting capacity is defined as:

$$N_{\text{struct}} = \sum_{k \in \mathcal{C}} \min(U_k, |\mathcal{J}_k|) \tag{38}$$

As previously calculated, $N_{\text{struct}} = 368$ chargers.

Solving the optimization model under a sufficiently large deployment limit confirms that the maximum feasible number of installable chargers equals 368, indicating that structural constraints, rather than electrical headroom, define the effective upper bound.

For comparison, the purely electrical (theoretical) capacity of the system is $N_{\text{theo}} = 409$ chargers. The difference between theoretical and structural capacity amounts to $N_{\text{theo}} - N_{\text{struct}} = 41$ chargers, representing electrical capacity that cannot be utilized due to insufficient candidate poles at certain cabinets.

This distinction highlights a key modelling insight:

- Electrical headroom alone does not determine effective hosting capacity;
- Spatial feasibility constraint must also be satisfied.

4.3.2. Maximum Installable Charging Power

At structural saturation, the maximum installable charging power equals:

$$P_{\text{max,struct}} = N_{\text{struct}} \cdot P_{\text{charger}}, \tag{39}$$

yielding $P_{\text{max,struct}} = 368 \times 3.68 = 1354.24$ kW, where $P_{\text{max,struct}}$ denotes the maximum installable charging power [kW].

This value represents the maximum slow AC charging power that can be integrated into the existing public lighting infrastructure under current spatial and electrical constraints.

The following table (Table 9) compares phased deployment levels with structural and theoretical limits.

Table 9. Comparison of deployment levels and infrastructure capacity limits.

Metric	Value
Theoretical electrical capacity N_{theo}	409 chargers
Structural hosting capacity N_{struct}	368 chargers
Phase 3 deployment	122 chargers
Phase 3 utilization of structural capacity	33%

The results indicate that even the large-scale rollout (122 chargers) utilizes only one-third of the structural capacity and less than 30% of the theoretical electrical capacity.

4.3.3. Infrastructure Stress Perspective

The interaction between deployment scale and structural capacity allows the identification of three distinct operating regimes:

$$\text{Regime I (Policy-limited):} \quad N_{\text{phase}} < N_{\text{struct}} \tag{40}$$

Deployment is constrained by external factors such as budgetary limits, implementation strategy, or political targets. Infrastructure capacity remains underutilized, and electrical feasibility does not restrict expansion.

$$\text{Regime II (Infrastructure-limited):} \quad N_{\text{phase}} \approx N_{\text{struct}} \tag{41}$$

Structural constraints become binding. All feasible candidate poles permitted by cabinet capacity are utilized. Further expansion within the existing lighting network becomes impossible without spatial modifications.

$$\text{Regime III (Infeasible):} \quad N_{\text{phase}} > N_{\text{struct}} \tag{42}$$

The requested deployment exceeds structural hosting capacity. Additional expansion would require:

- Installation of new poles;
- Reconfiguration of cabinet assignments;
- Grid reinforcement and capacity upgrades.

Under current rollout levels, the system operates clearly within Regime I, where deployment is constrained by policy rather than infrastructure capacity. The results confirm that present deployment levels remain substantially below structural saturation, indicating significant latent hosting capacity within the lighting network. However, full structural utilization would require installation at nearly all feasible candidate poles, reducing flexibility for future reallocation, redundancy, or demand redistribution. The identified structural capacity therefore establishes the upper technical bound against which regulatory adequacy under projected EV growth can be rigorously assessed in the subsequent section.

4.4. Policy Benchmarking Results

4.4.1. AFIR-Based Charging Power Requirement

The policy benchmarking framework introduced above is applied to evaluate the regulatory adequacy of lighting-integrated charging deployment.

According to the latest available statistics from the official vehicle registry database, the Croatian EV fleet consists of $N_{\text{BEV,HR}} = 9987$ battery electric vehicles and $N_{\text{PHEV,HR}} = 8146$ plug-in hybrid electric vehicles, yielding a total of $N_{\text{EV,HR}} = 18{,}133$ registered electric vehicles [34].

Since disaggregated city-level EV registration data were not publicly available at the time of analysis, the EV stock for Osijek was estimated by proportionally allocating national registrations using the demographic and vehicle fleet characteristics of the study area relative to the national average. The resulting baseline estimates are $N_{\text{BEV,OS}} = 290$ and $N_{\text{PHEV,OS}} = 235$.

While approximate, this allocation approach ensures structural consistency between national and city-level EV distributions. These values are used as the reference fleet size for AFIR-based benchmarking in the subsequent analysis. Applying the AFIR-based

formulation defined previously yields $P_{\text{AFIR}} = 565$ kW. Considering the slow charging proportion $\beta = 0.7$, the corresponding slow charging target equals $P_{\text{slow,target}} = 395.5$ kW.

4.4.2. Coverage Under Phased Deployment

Using the installed power values derived in the section above, the coverage indicator γ is computed (Table 10).

Table 10. AFIR slow charging coverage under current EV stock.

Scenario	Installed Power [kW]	γ
Phase 1	44.16	0.11
Phase 2	224.48	0.57
Phase 3	448.96	1.14

Under current EV penetration, the large-scale rollout (Phase 3) exceeds the slow charging benchmark, achieving 114% of the required capacity.

4.4.3. Projected Growth Scenario

To evaluate robustness under medium-term fleet growth, a threefold increase in EV stock is considered. The resulting charging target becomes $P_{\text{slow,target,2030}} = 1186.5$ kW, with a corresponding coverage indicator of $\gamma_{2030} = 0.38$.

The coverage indicator for 2030 indicates that lighting-integrated charging would cover only 38% of the projected requirement. It should be noted that this indicator corresponds to the Phase 3 deployment level; the implications under structural saturation are examined in the following subsection.

4.4.4. Structural Saturation Under Growth

At structural saturation, $P_{\text{max,struct}} = 1354.24$ kW, yielding $\gamma_{\text{struct,2030}} = 1.14$, indicating that from a spatial and cabinet-capacity planning perspective, compliance remains achievable under threefold growth but requires near-complete structural utilization.

4.4.5. Critical Penetration Threshold

The critical fleet growth multiplier at which lighting infrastructure alone ceases to satisfy the slow charging benchmark ($\gamma = 1$) is defined:

$$\gamma = \frac{P_{\text{max,struct}}}{P_{\text{slow,current}} \cdot m}, \tag{43}$$

$$P_{\text{max,struct}} = m_{\text{crit}} \cdot P_{\text{slow,current}}, \tag{44}$$

$$m_{\text{crit}} = \frac{P_{\text{max,struct}}}{P_{\text{slow,current}}}, \tag{45}$$

where m_{crit} denotes the critical EV fleet growth multiplier and $P_{\text{slow,current}}$ is the current slow charging target derived from AFIR [kW]. Substituting the computed values yields $m_{\text{crit}} = 1354.24/395.5 \approx 3.4$.

Beyond this multiplier, additional infrastructure expansion or grid reinforcement becomes necessary.

This analysis demonstrates that lighting-integrated infrastructure constitutes a technically robust but finite compliance resource. While sufficient under current conditions and moderate growth, structural saturation imposes a definable upper bound on regulatory adequacy.

4.4.6. Sensitivity Analysis of AFIR Benchmarking Assumptions

To assess the robustness of the compliance conclusions, two sensitivity analyses were conducted. Table 11 presents the effect of varying the slow-charging share parameter β. Table 12 examines the effect of varying the fleet growth multiplier.

Table 11. Sensitivity of AFIR coverage indicator γ to slow-charging share β (current EV fleet, Phase 3 and structural saturation).

β	$P_{\text{slow,target}}$ [kW]	γ (Phase 3)	γ (Structural)
0.5	282.5	1.59	4.79
0.7	**395.5**	**1.14**	**3.42**
0.9	508.5	0.88	2.66

Table 12. Sensitivity of AFIR coverage indicator γ to fleet growth multiplier ($\beta = 0.7$, Phase 3 and structural saturation).

Growth Multiplier	$P_{\text{slow,target}}$ [kW]	γ (Phase 3)	γ (Structural)
1×	395.5	1.14	3.42
2×	791.0	0.57	1.71
3×	**1186.5**	**0.38**	**1.14**
4×	1582.0	0.28	0.86

The results confirm that the baseline conclusions are robust under moderate variation of β. Phase 3 deployment satisfies the AFIR benchmark for $\beta \leq 0.7$, while structural saturation remains compliant across all tested values. With respect to fleet growth, structural saturation remains sufficient up to approximately 3.4× fleet growth. Beyond this threshold, additional infrastructure becomes necessary regardless of the slow-charging share assumption. In both tables, the bold row indicates the base case scenario: $\beta = 0.7$ in Table 11, and the fleet growth multiplier closest to the critical threshold ($m_{\text{crit}} \approx 3.4\times$) in Table 12.

4.5. Discussion

The results demonstrate that integrating slow AC charging infrastructure into existing public lighting networks represents a spatially and electrically viable at the planning level, and policy-relevant deployment pathway under current EV penetration levels. Beyond simple capacity quantification, the analysis reveals structural dynamics that provide broader methodological and planning insights.

4.5.1. Structural vs. Theoretical Hosting Capacity

A central contribution of this study is the explicit distinction between theoretical electrical capacity and effective structural hosting capacity. While cabinet-level ratings suggest a higher aggregate electrical potential, spatial feasibility constraints reduce the realizable deployment limit.

This finding demonstrates that grid-based assessments alone may systematically overestimate practical hosting capacity when spatial pole availability and cabinet–pole relationships are not explicitly modelled. The combined integration of electrical constraints with GIS-filtered candidate sets therefore represents a necessary methodological advancement toward realistic infrastructure reuse planning.

This structural–electrical coupling effect represents a second-order planning constraint that is typically neglected in feeder-level hosting capacity studies.

4.5.2. Deployment Regime Interpretation

The scenario analysis enables classification of deployment into three operational regimes: policy-limited, infrastructure-limited, and infeasible. Under current rollout scenarios, the system operates clearly within the policy-limited regime, where deployment scale is determined primarily by implementation strategy rather than electrical constraints.

This regime-based interpretation provides a transferable planning framework. It allows municipalities to identify whether expansion is constrained by infrastructure limits, regulatory benchmarks, or strategic rollout decisions, thereby reframing charging deployment as a structured optimization problem rather than a purely demand-driven expansion.

4.5.3. Regulatory Adequacy and Growth Robustness

Benchmarking against AFIR requirements indicates that lighting-integrated deployment can satisfy the slow-charging obligation under current EV penetration levels. However, medium-term fleet growth significantly alters this balance. While structural saturation remains sufficient up to a defined critical fleet multiplier, compliance under growth scenarios requires near-complete utilization of feasible candidate poles.

This demonstrates that public lighting infrastructure constitutes a robust but finite compliance resource. It can function effectively as a transitional or complementary deployment strategy, but long-term electrification planning must explicitly account for structural saturation thresholds.

4.5.4. Planning Implications

From a municipal planning perspective, the findings suggest that infrastructure reuse through public lighting integration offers:

- Accelerated deployment potential;
- Reduced civil works requirements;
- Distributed spatial coverage in residential zones.

However, reliance on full structural utilization reduces flexibility for redundancy, relocation, and future demand redistribution. Strategic planning should therefore balance short-term compliance benefits against long-term adaptability.

The proposed GIS–MILP–policy benchmarking framework provides a decision-support tool capable of quantifying these trade-offs prior to investment decisions.

Regarding traffic system reliability, slow AC charging stations integrated into public lighting poles operate exclusively within legally designated parking spaces. The act of parking a vehicle to charge is functionally identical to standard curbside parking and introduces no additional traffic disruption beyond what is inherent to the existing parking regime [21]. The traffic system impact is governed by the existing parking management framework rather than by the charging activity itself. No additional traffic reliability concerns therefore arise from the proposed infrastructure model.

Compared to conventional charging infrastructure deployment strategies, such as dedicated curbside chargers or private parking integration, the proposed approach offers a structurally distinct planning logic. Conventional strategies typically select a target location based on demand indicators and subsequently seek an electricity connection, often requiring new cable routing and civil works regardless of the installation context. The present framework inverts this logic: candidate locations are retained only where parking accessibility, proximity to demand generators, and cabinet-level electrical capacity simultaneously coincide. This dual filter—demand and supply simultaneously—reduces the risk of deploying infrastructure in locations that are either electrically infeasible or likely to remain underutilised, and represents a structural efficiency advantage over demand-only or supply-agnostic siting approaches. A full quantitative comparison against alternative

deployment strategies would require separate modelling efforts and is identified as a direction for future research.

From an implementation perspective, the practical availability of the proposed deployment pathway depends on three key preconditions. First, institutional coordination between municipal authorities and the public lighting operator is required to enable access to infrastructure data and physical pole modifications. Second, individual poles and cabinets must be technically verified against electrical and structural safety requirements prior to installation. Third, regulatory compliance with applicable safety standards and permitting procedures must be ensured. The GIS–MILP framework developed in this study provides the spatial and electrical screening necessary to support these preconditions, enabling municipalities to identify viable installation points before committing to detailed feasibility assessments.

4.5.5. Limitations and Future Research

Several limitations should be acknowledged. City-level EV stock was estimated due to the absence of disaggregated registry data, and simultaneity effects were represented using a fixed utilization factor α. Additionally, the analysis focused exclusively on slow AC charging and did not explicitly model reinforcement costs within the broader distribution network. While the reuse of existing public lighting infrastructure inherently avoids the civil works and grid connection costs associated with standalone charging deployment, thereby supporting the cost-effectiveness framing adopted in this study, a formal economic analysis quantifying these savings was not conducted and remains a priority for future research. A moderate power extension to 7.36 kW (single-phase Mode 2 charging) would remain feasible within the same infrastructure framework without requiring major grid reinforcement, representing a natural next step for extending the applicability of the proposed approach.

It should also be acknowledged that candidate pole availability may vary over time due to urban planning changes, pole replacements, or scheduled maintenance activities. The proposed framework is designed to be re-applicable as infrastructure data are updated, and periodic reassessment of the candidate set is recommended as part of a living decision-support process.

Future research may extend the framework by incorporating dynamic load modelling, stochastic charging behaviour, fast-charging infrastructure integration, economic cost optimization, and integration with medium-voltage grid constraints [35,36]. Grid load impacts, coincident loading scenarios, and active mitigation strategies such as smart charging and dynamic load shifting are addressed in the second stage of the research framework, namely the Dynamic Power Management component shown in Figure 1. This follow-up study is currently in preparation.

5. Conclusions

This study developed and applied a GIS-based multi-criteria optimization framework for allocating slow AC electric vehicle charging infrastructure integrated into existing public lighting networks. By combining spatial filtering, MCDA-based candidate ranking, cabinet-level electrical constraints, and MILP optimization, the proposed methodology enables realistic assessment of infrastructure reuse potential under phased deployment scenarios.

The results demonstrate that public lighting infrastructure can support substantial slow-charging deployment under current EV penetration levels. Applied to a real-world case study of 1223 feasible candidate poles across 160 public lighting cabinets in Osijek, Croatia, the framework identifies a structural hosting capacity of 368 chargers and a theoretical electrical capacity of 409 chargers. The difference of 41 chargers is attributed to spatial feasibility constraints at cabinet level. However, the analysis reveals that effective

hosting capacity is governed not only by aggregated electrical ratings but also by spatial feasibility constraints, which reduce the realizable deployment limit relative to theoretical capacity. This distinction between theoretical and structural hosting capacity represents a key methodological contribution of the study.

Benchmarking against AFIR regulatory requirements further shows that lighting-integrated charging can satisfy the slow-charging obligation under current fleet conditions. The large-scale deployment scenario (Phase 3, 122 chargers) achieves a coverage indicator of $\gamma = 1.14$, confirming regulatory adequacy under current EV penetration. However, under a projected threefold fleet growth, full structural utilization yields $\gamma_{\text{struct},2030} = 1.14$, indicating that compliance remains feasible only at near-complete infrastructure saturation. A critical fleet growth multiplier of $m_{\text{crit}} \approx 3.4$ defines the threshold beyond which public lighting infrastructure alone becomes insufficient to meet AFIR slow-charging requirements. Nevertheless, medium-term EV growth significantly alters this balance. While compliance remains achievable at the planning level up to a defined critical fleet multiplier, structural saturation establishes a measurable upper bound beyond which additional infrastructure expansion or grid reinforcement becomes necessary.

From a planning perspective, the findings indicate that public lighting integration offers an efficient transitional deployment strategy, characterized by reduced civil works and distributed residential coverage. The framework demonstrates that current deployment levels operate within a policy-limited regime, where scale is constrained by budgetary and strategic factors rather than electrical infrastructure capacity. Substantial latent hosting potential therefore remains available for near-term expansion without grid reinforcement. At the same time, reliance on near-complete structural utilization reduces flexibility for future system adaptation, underscoring the need for parallel long-term infrastructure planning.

Overall, the proposed GIS–MILP–policy benchmarking framework provides municipalities with a decision-support tool capable of quantifying electrical, spatial and regulatory constraints in an integrated manner. The framework advances the state of practice in urban EV charging infrastructure planning by explicitly linking spatial demand analysis, infrastructure-level electrical constraints, and regulatory compliance benchmarking within a single reproducible methodology. The resulting tool is transferable and applicable to other cities and public lighting networks. Future research may extend the approach by incorporating dynamic load behaviour, economic cost modelling, and integration with higher-voltage grid planning to support large-scale electrification scenarios.

Author Contributions: Conceptualization, J.P.; methodology, J.P.; software, J.P.; formal analysis, J.P.; investigation, J.P.; data curation, J.P.; writing—original draft preparation, J.P.; writing—review and editing, J.P. and D.T.; visualization, J.P.; supervision, D.T. All authors have read and agreed to the published version of the manuscript.

Funding: This work was supported through the financing of publication costs under Program Agreement No. 602-01/25-09/10 2158-60-02-25-18.

Informed Consent Statement: Not applicable.

Data Availability Statement: The spatial datasets used in this study were obtained from the City of Osijek and Promet i prostor d.o.o. The public lighting network data are not publicly available due to their sensitive nature as critical infrastructure. The optimization model code (Python/PuLP), derived candidate pole datasets with anonymized identifiers, aggregated cabinet-level capacity parameters, and MCDA suitability scores can be provided by the corresponding author upon reasonable request.

Acknowledgments: The authors would like to thank the City of Osijek and Promet i prostor d.o.o. for providing the spatial datasets used in this study. During the preparation of this manuscript, the authors used Claude 3.7 Sonnet (Anthropic, San Francisco, CA, USA) for coding assistance. The authors have reviewed and edited the output and take full responsibility for the content of this publication.

Conflicts of Interest: The authors declare no conflicts of interest.

Abbreviations

The following abbreviations are used in this manuscript:

AC	Alternating Current
AFIR	Alternative Fuels Infrastructure Regulation
BEV	Battery Electric Vehicle
CBC	Coin-or Branch and Cut
CRS	Coordinate Reference System
EPSG	European Petroleum Survey Group
EU	European Union
EV	Electric Vehicle
EVCS	Electric Vehicle Charging Station
GA	Genetic Algorithm
GIS	Geographic Information System
HTRS	Hrvatski Terrestrički Referentni Sustav
IQR	Interquartile Range
MCDA	Multi-Criteria Decision Analysis
MILP	Mixed-Integer Linear Programming
PHEV	Plug-in Hybrid Electric Vehicle
PSO	Particle Swarm Optimization
PuLP	Python Linear Programming
PV	Photovoltaic
QGIS	Quantum Geographic Information System
RWR	Rank-Weigh-Rank
TEN-T	Trans-European Transport Network
TM	Transverse Mercator

References

1. Singh, P.; Wen, F.; Palu, I.; Sachan, S.; Deb, S. Electric Vehicles Charging Infrastructure Demand and Deployment: Challenges and Solutions. *Energies* **2023**, *16*, 7. [CrossRef]
2. Unterluggauer, T.; Rich, J.; Andersen, P.B.; Hashemi, S. Electric vehicle charging infrastructure planning for integrated transportation and power distribution networks: A review. *eTransportation* **2022**, *12*, 100163. [CrossRef]
3. European Commission. Regulation (EU) 2023/1804 on the Deployment of Alternative Fuels Infrastructure. 2023. Available online: https://eur-lex.europa.eu/eli/reg/2023/1804/oj/eng (accessed on 1 February 2026).
4. Hardman, S.; Jenn, A.; Tal, G.; Axsen, J.; Beard, G.; Daina, N.; Figenbaum, E.; Jakobsson, N.; Jochem, P.; Kinnear, N.; et al. A review of consumer preferences of and interactions with electric vehicle charging infrastructure. *Transp. Res. Part D Transp. Environ.* **2018**, *62*, 508–523. [CrossRef]
5. Pan, L.; Yao, E.; Yang, Y.; Zhang, R. A location model for electric vehicle (EV) public charging stations based on drivers' existing activities. *Sustain. Cities Soc.* **2020**, *59*, 102192. [CrossRef]
6. Helmus, J.R.; Lees, M.H.; van den Hoed, R. A data driven typology of electric vehicle user types and charging sessions. *Transp. Res. Part C Emerg. Technol.* **2020**, *115*, 102637. [CrossRef]
7. Straka, M.; Piatrikóvá, L.; van Bokhoven, P.; Buzna, Ľ. A matrix approach to detect temporal behavioral patterns at electric vehicle charging stations. *Transp. Res. Procedia* **2021**, *55*, 1353–1360. [CrossRef]
8. Yaghoubi, E.; Yaghoubi, E.; Khamees, A.; Razmi, D.; Lu, T. A systematic review and meta-analysis of machine learning, deep learning, and ensemble learning approaches in predicting EV charging behavior. *Eng. Appl. Artif. Intell.* **2024**, *135*, 108789. [CrossRef]
9. Liu, J.; Peper, J.; Lin, G.; Zhou, Y.; Awasthi, S.; Li, Y.; Rehtanz, C. A planning strategy considering multiple factors for electric vehicle charging stations along German motorways. *Int. J. Electr. Power Energy Syst.* **2021**, *124*, 106379. [CrossRef]
10. De Gennaro, M.; Paffumi, E.; Martini, G. Customer-driven design of the recharge infrastructure and Vehicle-to-Grid in urban areas: A large-scale application for electric vehicles deployment. *Energy* **2015**, *82*, 294–311. [CrossRef]
11. Chen, Z.; Li, C.; Chen, X.; Yang, Q. Towards Optimal Planning of EV Charging Stations under Grid Constraints. *IFAC-PapersOnLine* **2020**, *53*, 14103–14108. [CrossRef]

12. Pengfei Zhao, A.; Li, S.; Li, Z.; Wang, Z.; Fei, X.; Hu, Z.; Alhazmi, M.; Yan, X.; Wu, C.; Lu, S.; et al. Electric Vehicle Charging Planning: A Complex Systems Perspective. *IEEE Trans. Smart Grid* **2025**, *16*, 754–772. [CrossRef]
13. Çelik, S.; Şeyda Ok. Electric vehicle charging stations: Model, algorithm, simulation, location, and capacity planning. *Heliyon* **2024**, *10*, e29153. [CrossRef]
14. Amin, A.; Tareen, W.U.K.; Usman, M.; Ali, H.; Bari, I.; Horan, B.; Mekhilef, S.; Asif, M.; Ahmed, S.; Mahmood, A. A Review of Optimal Charging Strategy for Electric Vehicles under Dynamic Pricing Schemes in the Distribution Charging Network. *Sustainability* **2020**, *12*, 10160. [CrossRef]
15. Cruz-Zambrano, M.; Corchero, C.; Igualada-Gonzalez, L.; Bernardo, V. Optimal location of fast charging stations in Barcelona: A flow-capturing approach. In Proceedings of the 10th International Conference on the European Energy Market (EEM), Stockholm, Sweden, 27–31 May 2013; pp. 1–6. [CrossRef]
16. Baouche, F.; Billot, R.; Trigui, R.; El Faouzi, N.E. Efficient Allocation of Electric Vehicles Charging Stations: Optimization Model and Application to a Dense Urban Network. *IEEE Intell. Transp. Syst. Mag.* **2014**, *6*, 33–43. [CrossRef]
17. Efthymiou, D.; Chrysostomou, K.; Morfoulaki, M.; Aifantopoulou, G. Electric vehicles charging infrastructure location: A genetic algorithm approach. *Eur. Transp. Res. Rev.* **2017**, *9*, 27. [CrossRef]
18. Matkovic, D.; Matijasevic, T.; Capuder, T. Charging station placement optimization based on the location significance prediction. *Energy Sources Part A Recover. Util. Environ. Eff.* **2024**, *46*, 12218–12239. [CrossRef]
19. Guerrero-Silva, J.A.; Romero-Gelvez, J.I.; Aristizábal, A.J.; Zapata, S. Optimization and Trends in EV Charging Infrastructure: A PCA-Based Systematic Review. *World Electr. Veh. J.* **2025**, *16*, 345. [CrossRef]
20. El-Bayeh, C.Z.; Zellagui, M.; Shirzadi, N.; Eicker, U. A Novel Optimization Algorithm for Solar Panels Selection towards a Self-Powered EV Parking Lot and Its Impact on the Distribution System. *Energies* **2021**, *14*, 4515. [CrossRef]
21. Zhang, R.; Kontou, E. Urban electric vehicle infrastructure: Strategic planning for curbside charging. *J. Transp. Geogr.* **2025**, *128*, 104328. [CrossRef]
22. European Commission Joint Research Centre. *Optimal Allocation of Electric Vehicle Charging Infrastructure in Cities and Regions*; European Commission Joint Research Centre: Brussels, Belgium, 2016.
23. Charly, A.; Thomas, A.; Vij, A.; Lyons, S. Identifying optimal locations for community electric vehicle charging. *Sustain. Cities Soc.* **2023**, *94*, 104573. [CrossRef]
24. Vafaei, N.; Ribeiro, R.; Camarinha-Matos, L. Normalization Techniques for Multi-Criteria Decision Making: Analytical Hierarchy Process Case Study. In *Technological Innovation for Resilient Systems*; Springer International Publishing: Cham, Switzerland, 2016. [CrossRef]
25. Gu, Y.; Celik, B.; Hachette, M.; Sechilariu, M.; Locment, F. Planning urban EV charging stations with GIS based multi-criteria decision making. *Power Electron. Devices Compon.* **2025**, *12*, 100132. [CrossRef]
26. Shen, W.; Zhou, B.; Jiang, R.; Shen, S. Sequential Charging Station Location Optimization under Uncertain Charging Behavior and User Growth. In Proceedings of the 2024 IEEE 63rd Conference on Decision and Control (CDC), Milan, Italy, 16–19 December 2024; pp. 2772–2777. [CrossRef]
27. Torkey, A.; Abdelgawad, H. Framework for planning of EV charging infrastructure: Where should cities start? *Transp. Policy* **2022**, *128*, 193–208. [CrossRef]
28. Wolsey, L.A. *Integer Programming*; Wiley: New York, NY, USA, 1998.
29. Sadeghi-Barzani, P.; Rajabi-Ghahnavieh, A.; Kazemi-Karegar, H. Optimal fast charging station placing and sizing. *Appl. Energy* **2014**, *125*, 289–299. [CrossRef]
30. Guler, N. Smart allocation and sizing of fast charging stations: A metaheuristic solution. *Int. J. Sustain. Energy* **2024**, *43*, 2350970. [CrossRef]
31. *IEEE Std C57.91-2011*; IEEE Guide for Loading Mineral-Oil-Immersed Transformers and Step-Voltage Regulators. IEEE: Piscataway, NJ, USA, 2011. [CrossRef]
32. Rancilio, G.; Bovera, F.; Delfanti, M. Slow but Steady: Assessing the Benefits of Slow Public EV Charging Infrastructure in Metropolitan Areas. *World Electr. Veh. J.* **2025**, *16*, 148. [CrossRef]
33. International Energy Agency. *Global EV Outlook 2023: Trends in Charging Infrastructure*; Technical Report; IEA: Paris, France, 2023.
34. Centar za vozila Hrvatske. *Registar Vozila—Statistički Podaci*; Centar za vozila Hrvatske: Zagreb, Croatia, 2024.
35. Matkovic, D.; Pilski, T.M.; Capuder, T. Participation of electric vehicle charging station aggregators in the day-ahead energy market using demand forecasting and uncertainty-based pricing. *Energy* **2025**, *328*, 136299. [CrossRef]
36. Wang, S.; Tan, Q.; Jiang, Q.; Shao, H.; Kouhi, M. Stochastic carbon-aware planning of renewable DGs and EV charging stations with demand flexibility in smart urban grids. *Sci. Rep.* **2025**, *15*, 34433. [CrossRef]

Disclaimer/Publisher's Note: The statements, opinions and data contained in all publications are solely those of the individual author(s) and contributor(s) and not of MDPI and/or the editor(s). MDPI and/or the editor(s) disclaim responsibility for any injury to people or property resulting from any ideas, methods, instructions or products referred to in the content.